RESEARCH ARTICLE

WILEY The Journal of Comparative Neurology

Proteomic analyses of nucleus laminaris identified candidate targets of the fragile X mental retardation protein

Hitomi Sakano[1] | **Diego A. R. Zorio[2]** | **Xiaoyu Wang[2]** | **Ying S. Ting[3]** | **William S. Noble[3]** | **Michael J. MacCoss[3]** | **Edwin W Rubel[1]** | **Yuan Wang[2,4]**

[1]Virginia Merrill Bloedel Hearing Research Center, Department of Otolaryngology-Head and Neck Surgery, University of Washington, School of Medicine, Seattle, Washington

[2]Department of Biomedical Sciences, Florida State University, Tallahassee, Florida

[3]Department of Genome Sciences, University of Washington, Seattle, Washington

[4]Program in Neuroscience, Florida State University, Tallahassee, Florida

Correspondence
Yuan Wang, Department of Biomedical Sciences, Florida State University, 1115 West Call Street Tallahassee, FL 32306.
Email: yuan.wang@med.fsu.edu

Abstract

The avian nucleus laminaris (NL) is a brainstem nucleus necessary for binaural processing, analogous in structure and function to the mammalian medial superior olive. In chickens (*Gallus gallus*), NL is a well-studied model system for activity-dependent neural plasticity. Its neurons have bipolar extension of dendrites, which receive segregated inputs from two ears and display rapid and compartment-specific reorganization in response to unilateral changes in auditory input. More recently, fragile X mental retardation protein (FMRP), an RNA-binding protein that regulates local protein translation, has been shown to be enriched in NL dendrites, suggesting its potential role in the structural dynamics of these dendrites. To explore the molecular role of FMRP in this nucleus, we performed proteomic analysis of NL, using micro laser capture and liquid chromatography tandem mass spectrometry. We identified 657 proteins, greatly represented in pathways involved in mitochondria, translation and metabolism, consistent with high levels of activity of NL neurons. Of these, 94 are potential FMRP targets, by comparative analysis with previously proposed FMRP targets in mammals. These proteins are enriched in pathways involved in cellular growth, cellular trafficking and transmembrane transport. Immunocytochemistry verified the dendritic localization of several proteins in NL. Furthermore, we confirmed the direct interaction of FMRP with one candidate, RhoC, by in vitro RNA binding assays. In summary, we provide a database of highly expressed proteins in NL and in particular a list of potential FMRP targets, with the goal of facilitating molecular characterization of FMRP signaling in future studies.

KEYWORDS
autism spectrum disorders, cytoskeletal proteins, dendritic plasticity, gene ontology, RNA binding protein, RhoC, RRID: AB_94856, RRID: AB_776174, RRID: AB_297884, RRID: AB_357520, RRID: AB_309663, RRID: AB_2277755, RRID: AB_2155806, RRID: AB_1859928, RRID: AB_10615780, RRID: AB_2620155

1 | INTRODUCTION

Local translation of mRNAs occurs in dendrites in response to changes in neuronal activity (Martin & Zukin, 2006; Steward & Falk, 1985;

Steward, Farris, Pirbhoy, Darnell, & Driesche, 2014). Fragile X mental retardation protein (FMRP) is an RNA binding protein, which plays an important role in proper dendrite development by mechanisms of local translation (Santoro, Bray, & Warren, 2012). Loss of FMRP leads to fragile X syndrome (FXS), a neurodevelopmental disorder with sensory, learning, and social difficulties (Penagarikano, Mulle, & Warren, 2007). We have yet to understand the exact mechanism underlying these difficulties, but evidence suggests that abnormal dendritic plasticity is involved. Postmortem analyses of the brains of FXS patients as well as knock-out animal models reveal abnormalities of dendrites (Galvez, Gopal, & Greenough, 2003; Galvez & Greenough, 2005; Hinton,
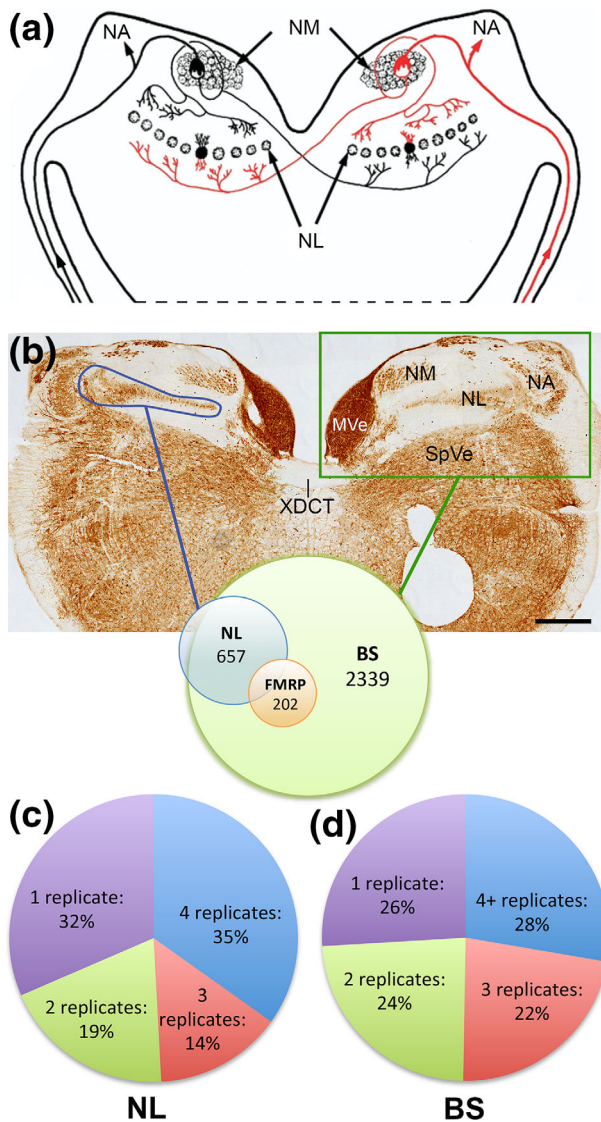

Abbreviations: eEF1a, eukaryotic elongation factor 1a; eEF2, eukaryotic elongation factor 2; MAP1B, microtubule-associated protein 1B; MAP2, microtubule-associated protein 2; Mve, medial vestibular nucleus; NM, nucleus magnocellularis; NL, nucleus laminaris; NA, nucleus angularis; SpVe, spinal vestibular nucleus; SERCA, arco/endoplasmic reticulum Ca^{2+}-ATPase; TuJ-1, neuron-specific class III beta-tubulin; XDCT, dorsal crossed cochlear track.

FIGURE 1 Proteins identified from nucleus laminaris (NL) and dorsal brainstem (BS). (a) Schematic of a coronal section of the brainstem is shown. Signals from the cochlea are transmitted via the eighth cranial nerve to NM. NM neurons then project to the dorsal aspect of ipsilateral NL and decussate to target the ventral aspect of contralateral NL. Axons and neurons innervated by the right cochlea are indicated in red color. (b) A low-magnification image taken from the caudal brainstem at the level of NL in the coronal plane. The section is immunostained for microtubule-associated protein 2 (MAP2) to illustrate the location of the cell groups. Proteomic analysis was performed on unstained tissue block containing auditory brainstem (green box) or just NL collected by laser microdissection of cryosections (blue lines). 657 proteins identified from NL are a subset of 2,339 proteins identified from BS. 202 proteins are putative FMRP targets. (c, d) Pie charts demonstrate the distribution of identified proteins from NL (c) and BS (d) that were identified in one, two, three or four biological samples. Abbreviations: NM, nucleus magnocellularis; NL, nucleus laminaris; NA, nucleus angularis; MVe, medial vestibular nucleus; SpVe, spinal vestibular nucleus; XDCT, dorsal crossed cochlear track. Scale bars = 500 μm in (a) [Color figure can be viewed at wileyonlinelibrary.com]

Brown, Wisniewski, & Rudelli, 1991; Irwin, Galvez, & Greenough, 2000; Zarnescu, Shan, Warren, & Jin, 2005).

We have previously shown that FMRP is enriched in the dendrites of chick nucleus laminaris (NL) as well as in its equivalent structure, the medial superior olive (MSO), in mammals, including humans (Wang et al., 2014). NL and MSO are important for detecting temporal coincidence of afferent input between the two ears, which is believed to be essential for encoding the location of sound source along the azimuth (reviewed in Ashida & Carr, 2011; Grothe, 2000; Joris & Yin, 2007; Kuba, 2007). As a fundamental substrate for computing interaural time differences (ITDs), NL and MSO neurons form bipolar dendrites that are innervated differentially by segregated afferent inputs from the two ears. The evolutionary conservation in FMRP expression in NL and MSO dendrites suggests its importance in auditory temporal processing. Consistently, FXS patients exhibit problems with communication, hypersensitivity to auditory stimuli and inability to habituate to repeated auditory stimuli (Rotschafer & Razak, 2014). FMRP knock-out mice also display hypersensitivity to auditory stimuli (Chen & Toth, 2001).

NL/MSO dendrites display compartment-specific plasticity in structure and in protein levels, consistent with the functional role of FMRP in regulating dendritic and synaptic modifications via spatially controlling translation of its mRNA targets. Dendrites of NL and MSO neurons are highly dynamic. For example, unilateral deafening causes retraction of the dendrites receiving input from the affected side but not the other dendrites of the same neurons (Benes, Parks, & Rubel, 1977; Deitch & Rubel, 1984). Changes in dendrites, including the shortening of terminal dendritic branches, occur rapidly, within hours, and importantly, these changes are reversible in response to changes in afferent activity (Sorensen & Rubel, 2006, 2011; Wang & Rubel, 2012). Accompanying the structural changes, altered expression levels of a number of proteins in these dendrites also occur within a similar timescale (Wang & Rubel, 2008). These rapid and highly localized changes suggest that very rapid mechanisms are taking place perhaps by local protein translation or degradation.

Thus, NL/MSO provides a suitable model for studying neuroplasticity in dendrites, particularly for studying the molecular and cellular events regulated by FMRP signaling, with functional and clinical relevance to understanding the auditory and communication related behavioral deficits in FXS. Several hundred potential mRNA targets of FMRP have been predicted from tissue samples homogenized from whole mouse brains (Brown et al., 2001; Darnell et al., 2011; Ascano et al., 2012). In the current study, we take advantage of the simple anatomy of the chicken NL, which allows for the specific tissue collection from one neuronal cell type and its incoming afferent axons (Figure 1). We first identified the proteins expressed in NL by mass spectrometry using a shotgun proteomic approach and then performed comparative analyses to identify potential FMRP targets in NL. In addition, we verified the dendritic localization of a number of the identified candidates using immunocytochemistry and confocal imaging. Finally, we confirmed the direct interaction of one such candidate with FMRP using in vitro RNA electrophoretic mobility shift assay (REMSA). Our results provide a list

of promising FMRP targets in NL dendrites that may be important to structural dynamics of NL dendrites.

2 | MATERIALS AND METHODS

This study was performed on White Leghorn chick hatchlings (*Gallus gallus*) of less than 10-day age. All procedures were approved by the Florida State University and University of Washington Institutional Animal Care and Use Committees, and carried out in accordance with the National Institutes of Health Guide for the Care and Use of Laboratory Animals.

2.1 | Tissue collection for mass spectrometry

Two types of tissue samples were collected from the brainstem of newly hatched chickens (postnatal day 0–4; $n = 18$ total). The first sample type was collected specifically from the NL cell group (Figure 1b; blue lines). After decapitation, the brains were quickly removed from the skull. The brainstem was blocked and immersed in optimal culture temperature (OCT) compound (Thermo Scientific, Inc., Waltham, MA), snap frozen in liquid nitrogen and stored at −80°C. Coronal sections (20 μm thick) containing NL were collected from the brainstem block using a cryostat and mounted on 0.9 μm Polyesther (POL)-membrane slides (Leica Microsystems, Buffalo Grove, IL). Under a laser micro-dissection microscope (LMD-6000; Leica Microsystems), the NL was outlined at 20× magnification, containing cell bodies and dendritic layers of NL with minimal inclusion of surrounding tissues. The outlined tissue was dissected with a laser (laser line width of 2 μm; laser power at 128, cutting speed at 1 μm per section) and dropped into a sterile 0.6 ml microtube. Dissected NL pieces from both sides of the brainstem from two animals were combined in one microtube and considered as one biological sample labeled as "NL". In total, we collected four NL biological samples from eight animals. These samples were stored at −80°C until protein extraction. The number of animals needed was based on how much protein was needed to identify ∼500–2,000 proteins.

The second type of tissue sample was collected from the dorsal brainstem at the caudorostral level of NL (Figure 1b; green lines). After the brain was removed from the skull, a 3 mm thick block was manually collected from the brainstem and placed flat in a petri dish. The dorsal brainstem at the level of the crossed dorsal cochlear tract was separated from the ventral brainstem. This sample contains three auditory nuclei (NL, nucleus magnocellularis, and nucleus angularis) as well as several vestibular cell groups (medial, lateral, spinal, and ventral vestibular nuclei). Similarly, tissue samples from two animals were combined as one biological sample labeled as "BS" (brainstem). In total, we collected five BS biological samples from ten animals. These samples were snap frozen in OCT in liquid nitrogen and stored at −80°C until protein extraction.

2.2 | Protein preparation for mass spectrometry

For BS samples, tissues were thawed on ice in T-buffer (20 mM Tris, 150 mM NaCl, 1 mM EDTA, 1 mM EGTA), sonicated in 2 × 10 s pulses in 500–1000 μl volume, centrifuged at 2,300 × g for 10 min to remove cellular debris. Supernatant was diluted to 1 mg/ml and then

ultracentrifuged at 100,000 × g for 1 hr. To improve the identification of low abundance membrane proteins, the membrane pellet and cytosolic supernatant were collected separately and processed independently as one biological sample each. Both were solubilized at 60°C in sodium dodecyl sulfate (SDS) at a final concentration of 0.1%, incubated in 5 mM dithiothreitol (DTT) for 30 min at 60°C followed by 15 mM Iodoacetamide (IAA), an alkylating agent, for 30 min at the room temperature in the dark, and then digested with 2 μg trypsin (Sigma, proteomic grade) overnight at 37°C to hydrolyze specifically at the carboxyl side of arginine and lysine residues. Samples were hydrolyzed with 100 mM HCl for 5 min at 37°C. Detergent was then removed with Oasis MCX cleanup kit (Waters Corporation; Milford, MA).

For NL samples which were attached to POL membrane pieces, samples were incubated with 0.1% rapigest/Tris-buffer for 5 min at 95°C. As described above, tissues were treated with DTT and IAA. Proteins were digested with trypsin and then the detergent was hydrolyzed with HCl. Samples were centrifuged twice at 16,000 × g for 5 min each to remove the POL membrane debris. The solution was dried to a volume of 20 μl with a speedvac before mass spectrometry.

2.3 | Mass spectrometry (MS) and protein identification

Purified peptide samples were loaded onto 30 cm by 75 μm width silica columns packed with 4 μm Jupitor 90Å beads and 2 mm length Kasil trap with 3 μm Jupitor 90Å beads. Flow pressure was kept ∼1,500 psi at 0.250 μl/min flow. The LTQ-FT Ultra (ThermoFisher Scientific) mass spectrometer was used. Spectra were acquired using a cycle of one high-resolution MS scan (400–1400 m/z) followed by five data-dependent MS/MS scans at low resolution, repeated continuously throughout the analysis. Spectra were matched to peptide sequences using SEQUEST (Eng, McCormack, & Yates, 1994) (non-tryptic ends). Peptide-spectrum match (PSM) and peptide identifications were obtained from Percolator (v2.01) (Käll, Canterbury, Weston, Noble, & MacCoss, 2007). Peptides with Percolator with q-value <0.01 were given as input to ID Picker (Zhang, Chambers, & Tabb, 2007) for protein identification. We used a decoy database using scrambled *Gallus gallus* genome sequence (build 12/17/11). We required at least 2 peptides per protein, each with a q-value (false discovery rate) of <0.01 (estimated 1% rate of false discoveries among the accepted peptides). At least four biological replicates with three technical replicates each were performed. We required each peptide to present in every technical replicate ($n = 3$) and at least 2 peptides per protein for identification. Because of the multiple technical replicates, we pooled the proteins identified in each of the biological samples. Figure 1c, d demonstrates the percentages of proteins identified in multiple biological samples. Protein identification comparisons among different experiments were made using MSDaPl (Sharma, Eng, MacCoss, & Riffle, 2012).

2.3.1 | Gene ontology analyses

Several software programs were used to perform gene ontology analyses of the identified proteins. The first is the DAVID Bioinformatics Resources 6.8 (National Institute of Allergy and Infectious Diseases,

TABLE 1 Primary antibodies used for immunocytochemistry and other staining

	Immunogen	Manufacturer, catalog number, Host, monoclonal or polyclonal; RRID,	Concentration
Anti-MAP2	Bovine brain MAP2 (aa 997–1332)	Millipore (Billerica, MA), MAB3418; Mouse monoclonal; RRID:AB_94856	1:1,000 (ICC); 1:1,000 (WB)
Anti-MAP2	Synthetic peptide rat MAP2 (aa 1-100)	Abcam (Cambridge, MA), ab32454; Rabbit polyclonal; RRID:AB_776174	1:1,000 (ICC)
Anti-MAP1B	Full length rat brain MAP1B	Abcam, Ab11266; Mouse monoclonal IgG1 clone AA6; RRID:AB_297884	1:10,000 (ICC); 1:1,000 (WB)
Anti-TuJ-1	Rat brain tubulin beta-3	R&D Systems (Minneapolis, MN), MAB1195; Mouse monoclonal IgG2a; RRID:AB_357520	1:10,000 (ICC); 1:1,000 (WB)
Anti-eEF1a	Crude calmodulin-binding proteins from Trypanosoma brucei chromatography	Millipore, 05–235; Mouse monoclonal IgG1k clone CBP-KK1; RRID:AB_309663	1:1,000 (ICC); 1:1,000 (WB)
Anti-p-eEF2	Synthetic phosphopeptide surrounding Thr56 of human eEF2, GETRFtDTRK	Cell Signaling Technology (Danvers, MA), No. 2331; Rabbit polyclonal; RRID:AB_2277755	1:1,000 (ICC)
Anti-NSF-1	Recombinant human full length NSF.	Abcam, ab16681; Mouse monoclonal IgG; RRID:AB_2155806	1:1,000 (ICC); 1:1,000 (WB)
Anti-RhoC	Synthetic peptide human RhoC (aa 100-C-term)	Abcam, ab64659; Rabbit polyclonal; RRID:AB_1859928	1:1000 (ICC); 1:1000 (WB)
Anti-SERCA2	Purified canine cardiac sarcoplasmic reticulum.	Millipore, MAB2636; Mouse monoclonal IgG1k clone IID8; RRID:AB_10615780	1:1,000 (ICC); 1:1,000 (WB)

Abbreviations: ICC: immunocytochemistry; WB: Western blot.

National Institute of Health; https://david.ncifcrf.gov/). We used this resource for protein functional annotation and gene ID conversion. Ensembl Bio-mart software (http://www.ensembl.org/biomart/mart-view/) was also used for gene ID conversion. For identifying transmembrane proteins, we used the TMHMM program version 2.0 located at: http://www.cbs.dtu.dk/services/TMHMM/. Finally, we used the Ingenuity pathway analysis at http://www.ingenuity.com/as an alternative approach to DAVID for identifying enriched pathways.

2.4 | Western blot

Protein samples were harvested from flash frozen chicken brainstem tissue. Samples were homogenized in EDTA buffer (62.5 mM Tris-HCl pH 6.8, 2% SDS, 10% Glycerol, 5% β-ME, 10 mM EDTA) using the Ultra-Turrax® T10 homogenizer (IKA® Works, Inc., Wilmington, NC). 50 μg of protein lysate in SDS buffer (2% SDS, 50 mM Tris pH 7.6, 5% glycerol, and 0.025% bromophenol blue) was incubated at 70°C for 10 min, resolved in NuPAGE 4–12% Bis-Tris Gels (Life Technologies, Carlsbad, CA), and then transferred onto PDVF membranes (GE Healthcare, Chicago, IL). After blocking in 5% milk in PBS with 0.05% Tween (PBS-T) for 30 min at room temperature, membranes were probed against the primary antibodies (Tab. 1) overnight at 4°C in 1% milk in PBS-T. Specific secondary HRP-conjugated antibodies were used at 1:2,500 dilutions (Santa Cruz, Biotechonology®, Inc., Dallas, TX) and blots were developed with SuperSignal™ West Pico

Chemiluminescent Substrate (Thermo Scientific, Inc., Waltham, MA) and exposed to X-ray film.

2.5 | Immunostaining

Immunocytochemistry was used to verify the expression of a number of MS-identified proteins in NL neurons and examine their subcellular localization. Chickens (P0–P4) were transcardially perfused with 0.9% saline followed by 4% paraformaldehyde in 0.1 M phosphate buffer (PB). The brains were removed from the skull, post fixed overnight in the same fixative, and transferred to 30% sucrose in 0.1 M PB. Brains were then sectioned in the coronal plane at 20–30 μm on a freezing sliding microtome or a cryostat and collected in PBS. Sections containing NL were immunostained using the primary antibodies listed in Table 1. The staining procedure was described previously (Wang, Cunningham, Tempel, & Rubel, 2009). Briefly, blocking was performed by 4% normal goat serum in PBS overnight at 4°C or with a blocking solution (PerkinElmer FP1020; Waltham, MA) at room temperature for 30 min. Sections were incubated with primary antibody solutions diluted in PBS with Triton X-100 (at a concentration of 0.3% or 0.5%) overnight at 4°C followed by AlexaFluor secondary antibodies (1:200) for 1–2 hr at room temperature. Secondary antibodies were purchased from either Molecular Probes (Eugene, OR) or Jackson ImmunoResearch (West Grove, PA). Sections were coverslipped with Fluoromount-G (SouthernBiotech, Birmingham, AL).
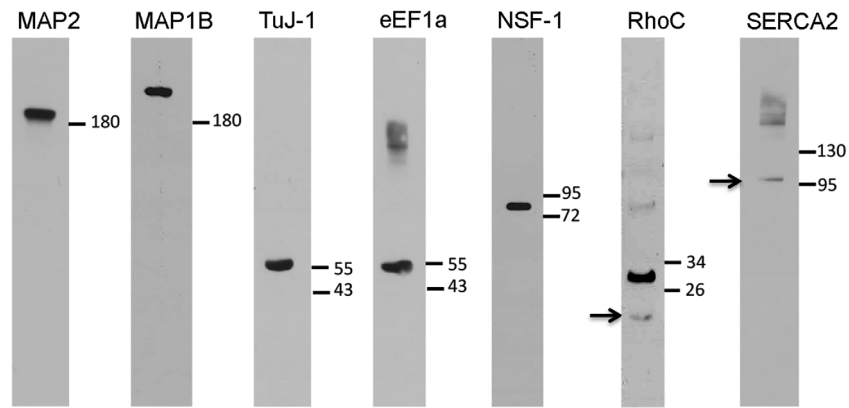
FIGURE 2 Western blotting for antibody characterization in the chicken brain. Fifty micrograms (μg) of protein lysate from brain tissue was loaded to each lane. Molecular weight standards (right to each lane) were used to determine relative sizes of labeled protein bands. Arrows point to the bands of the protein of interest with predicted molecular weight. See Table 1 and the Methods for more information on these antibodies

2.6 | Antibody characterization

Table 1 lists the primary antibodies used in the current study, including the immunogen, host species, clone type, manufacturer's information, as well as dilution used for each antibody.

We used the microtubule-associated protein 2 (MAP2) as a dendritic marker. MAP2 expression and immunohistochemistry using a mouse monoclonal antibody (Millipore, MAB3418) in NL dendrites has been well characterized (Wang & Rubel, 2008; Wang et al., 2014). In this study, we also used a second rabbit polyclonal antibody for MAP2 (Abcam, ab32454) to facilitate double staining with other antibodies raised in the mouse. Double staining with both the rabbit and mouse anti-MAP2 antibodies demonstrated identical staining pattern in NL (see Figure 5). In this study, we verified the specificity of the mouse anti-MAP2 antibody with Western blot in chicken brain tissue (Figure 2).

Mouse monoclonal anti-MAP1B (clone AA6) was produced using rat brain MAP. This antibody recognizes a conserved nonphosphorylated and nonphosphorylatable epitope on MAP1B (DiTella, Feiguin, Carri, Kosik, & Cáceres, 1996; Paglini et al., 1998). It reacts with all isoforms of MAP1B, in both Western blot and immunofluorescence applications (Franzen et al., 2001; Impens et al., 2008; Eriksson et al., 2010). Based on the datasheet provided by the manufacturer, this antibody does not react with tubulin or other microtubule associated proteins. In chicken brain tissue, we verified the specificity of the antibody recognizing the chicken MAP1B protein by western blot (Figure 2).

The clone TuJ-1 of the anti-beta-III tubulin monoclonal antibody was raised against rat microtubules and purified from hybridoma culture supernatant. This antibody recognizes neuron-specific beta-III tubulin specifically, as verified by both Western blot and immunocytochemistry in human, mouse, and rat brains (see the datasheet provided by the manufacturer). In this study, we further verified the specificity of the antibody in chicken brain tissue, demonstrating a single Western blot band at approximately 55 kDa (Figure 2), the predicted molecular weight for chicken beta-III tubulin.

The clone CBP-KK1 of the anti-eEF1a monoclonal antibody was produced against crude calmodulin-binding proteins from *Trypanosoma brucei* (*T. brucei*) isolated using calmodulin-affinity chromatography. This antibody binds to eEF1 alpha by lambda library from *T. brucei* (Kaur & Ruben, 1994). In this study, we confirmed that the antibody recognizes the chicken eEF1a at ~50 kDa protein (Figure 2), corresponding to the predicted molecular weight.

The anti-phosphorylated-eEF2 (anti-p-eEF2) antibody was raised against the phosphor peptide surrounding Thr56 of human eEF2. We have previously characterized this antibody by Western blot in chicken brain samples (McBride, Rubel, & Wang, 2013). This anti-p-eEF2 antibody recognizes chicken p-eEF2 at ~95 kDa.

Monoclonal antibody to NSF protein was raised against recombinant human NSF and previously characterized by Western blotting (Boström et al., 2007). In this study, we identified a single band at approximately 80 KDa on Western blot for the chicken brain tissue (Figure 2), corresponding to the predicted molecular weight.

Anti-RhoC rabbit polyclonal antibody was raised against the synthetic peptide corresponding to the C-terminal end (aa100-C-term) of human RhoC. The manufacturer tested the antibody in human and mouse cells by Western blot. In this study, we verified that this antibody recognizes a 21 kDa band on Western blotting (Figure 2), corresponding to the predicted chicken RhoC protein. In addition, there is a second, strong unexpected band of higher molecular weight at ~30 kDa.

The IgG1k clone IID8 of the anti-SERCA2 monoclonal antibody was developed against canine cardiac sarcoplasmic reticulum and recognizes human SERCA2 (Chami et al., 2001). In this study, we confirmed the specificity of the antibody in the chicken brain by Western blot, showing a band of approximately 105 kDa (Figure 2), corresponding to the predicted molecular weight of the chicken SERCA2.

2.7 | Phalloidin staining

Phalloidin is a well characterized chemical used for staining filamentous actin (F-actin). Following immunocytochemistry for a MAP2 antibody, the sections were incubated in Alexa Fluor 647 Phalloidin (Life Technology; Eugene, OR) diluted in 1:100 in PBS for 30 min in the dark at the room temperature. Staining was stopped by washing the sections in PBS.

2.8 | Imaging

Images were captured either with a Zeiss M2 microscope for bright-field and epi-fluorescent images, or with the Zeiss LSM 880 confocal microscope. Epi-fluorescent images taken with the M2 microscope were treated with the Zeiss Apotome, an optical sectioning approach using structured illumination for reducing out-of-focus information in epi-fluorescent images (Neil, Juskaitis, & Wilson, 1997; Neil, Squire, Juskaitis, Bastiaens, & Wilson, 2000). Photomontages were applied in the Zeiss Zen blue software. Image brightness, gamma, and contrast adjustments were performed in Adobe Photoshop (Adobe Systems, Mountain View, CA). All adjustments were applied equally to all images of the same set of staining from the same animal unless stated otherwise.

2.9 | Recombinant chicken HIS tagged FMRP expression and purification

Chicken FMRP isoform 2, sequence-optimized for expression in *Escherichia coli*, was cloned into the NdeI/XhoI restriction sites in the expression vector pET-21a (+) (Merck Millipore Corp., Billerica, MA) containing a histidine (His) tag. BL21 *E. coli* cells were transformed via electroporation and glycerol stocks were stored at −80°C. Cells were plated on 2YT/Amp plates and incubated for 16 hr at 37°C. 1 L of 2YT/Amp culture was inoculated from fresh confluent plate and grown to OD_{595} between 0.6 and 0.7 at 37°C with vigorous shaking. Isopropyl β-D-1-thiogalactopyranoside (IPTG) was added to final concentration of 1 mM and cells were grown at 30°C with vigorous shaking for 3 hr. Cells were pelleted by centrifugation at 4,000 rpm for 15 min at 4°C. Cell pellets were resuspended in Lysis buffer (20 mM HEPES pH 7.5, 200 mM NaCl, 10 mM β-mercaptoethanol, 25 mM Imidazole) plus protein inhibitors: 0.5 mM PMSF, 2μg/mL of Aprotinin, 0.5 μg/mL of Leupeptin and 1 μg/mL of Pepstatin, frozen in dry ice and stored at −80°C freezer. Cells were thawed at 37°C and kept on ice for 15 min. Protease inhibitors were added and Bugbuster® plus Lysonase (Merck Millipore) were added and incubated at 4°C for 20 min in a nutator. Triton X-100 was added to final concentration of 1% and incubated for 10 min at 4°C in the nutator. Cell lysate was centrifuged at 15,000 × g for 30 min at 4°C. Supernatant was added to 1 mL of Ni-NTA resin (Qiagen, Inc., Hilden, Germany) pre-washed in lysis buffer and batch binding was performed at 4°C for 2 hr. Resin was washed with 40 volumes of Lysis buffer plus 0.5% NP40 and resuspended in 40 vol of Lysis buffer containing 40 mM of Imidazole. The ressuspended beads were added to a column and settled by flow gravity. His-FMRP protein was eluted with 4 × 1 mL of Lysis buffer plus 100 mM Imidazole. Eluates were pooled and dialyzed against dialysis buffer (20 mM HEPES pH 7.5, 1 mM EDTA, 2 mM DTT, 100 mM NaCl, 0.05% NP40 and 20% Gycerol). Protein concentration was measured using standard techniques, aliquoted and stored at 4°C.

2.10 | RNA gel electrophoretic mobility shift assay

To test for direct interaction between FMRP and RhoC, we looked at the RNA sequence for RhoC and identify several of putative FMRP binding domains based on previous work by Anderson, Chopra, Suhl, Warren, and Bassel (2016). We then chose a region that contained at least six putative binding sites and designed an RNA probe for RhoC containing these putative binding sites. The 5′ biotin-labeled and unlabeled RhoC RNAs were chemically synthesized (GenScript, Picataway NJ) with the following sequence: 5′ GAACUACAUCGCCGACAUU-GAGGUGGAUGGGAAGCAGGUGGAGCUGGCG −3′. RNA binding was carried out using the LightShift® Chemiluminescent RNA EMSA kit (Thermo Fisher Scientific, Waltham, MA). Briefly, 5 mM of biotin-labeled RhoC RNA was incubated with 125 ng of purified HIS-FMRP in the absence or presence of increasing concentrations of unlabeled RhoC RNA as well as with increasing concentrations of a non-specific unlabeled RNA probe, for 30 min at room temperature. The reactions were electrophoresed in 6% polyacrylamide gel in 0.5X Tris Borate EDTA (TBE) and transferred onto a nylon membrane. Blot was UV cross-linked at 120 mJ/cm^2 using a CL-1000 UV Cross linker (UVP LLC, Upland, CA). Blot was blocked, probed with Streptavidin-Horseradish Peroxidase conjugate, and exposed to X-ray film.

3 | RESULTS

3.1 | Identification of proteins from dorsal brainstem (BS) and NL

Using mass spectrometry, we identified 657 proteins from four biological samples of NL (blue, NL laser capture) (Figure 1b). Approximately two thirds of these proteins (450; 68%) are identified in more than one biological replicates and more than one third of total proteins (229; 35%) are identified in all four biological replicates (Figure 1c). The total spectral count for and the number of biological replicates in which each protein was identified are listed in Supporting Information Table S1.

Although laser capture provides specificity of tissue collection from NL, we needed to verify that the additional steps in tissue processing do not cause a significant increase in false positives. A comparison with traditional approach of snap frozen tissue served as a straightforward and powerful strategy to address this issue. We identified 2,339 proteins from five biological samples of BS (green, dorsal brainstem en bloc; snap frozen tissue, Figure 1b). Among these proteins, 1,732 (74%) proteins are identified in more than one biological replicates and 648 (28%) proteins are identified in at least 4 out of 5 biological replicates (Figure 1d), demonstrating comparable reproducibility as NL samples. The total spectral count for and the number of biological replicates in which each protein was identified, are listed in Supporting Information Table S2. The majority (96%; 632/657) of NL proteins were also identified in BS. This near complete overlap is consistent with NL proteins being a subset of BS proteins and further validates the reproducibility of the protein identification strategy.

On the other hand, a number of proteins that are known to be expressed in NL neurons were not identified in NL samples but included in BS proteins, such as FMRP itself, indicating that the 657 protein list of NL is only a fraction of the entire proteomics of this nucleus. Using the THMM software, we found 13% of NL and 20% of BS proteins with predicted transmembrane features. As a comparison,

TABLE 2 Enriched pathways of NL and BS proteins revealed by DAVID analysis

	Nucleus Laminaris (NL)			Dorsal Brainstem (BS)	
	Cluster	Enrichment Score		Cluster	Enrichment Score
1	Mitochondrial	16.28	1	Mitochondrial	12.50
2	Ribosomal/Translation	13.98	2	Metabolic	12.24
3	Protein folding	9.94	3	Ribosomal/Translation	9.48
4	Cytoskeletal	9.18	4	Respiration	7.49
5	Metabolic	9.08	5	Oxidative	7.29
6	Protein transport	8.79	6	Protein folding	6.39
7	Cellular respiration	8.21	7	Nucleotide binding	5.95
8	Nucleotide binding	7.37	8	Cytoskeletal	5.89
9	Neuronal projection	7.12	9	Nucleotide binding	5.09
10	RNA recognition	6.69	10	Oxidoreductase	4.97

Proteins identified from each tissue set were compared to the genome of *Gallus gallus* to determine if there is enrichment for proteins from certain pathways, using DAVID program. Score of >1.3 is significant. The top five enriched pathways suggest a highly metabolic mileu.

human genome predictions have estimated ∼20% are transmembrane proteins, suggesting that our proteomic analysis of NL may be biased towards soluble proteins. In support of this suggestion, NL neurons express a number of voltage-gated potassium and sodium channels as evidenced by previous immunocytochemical studies (Lu, Monsiavis, Tempel, & Rubel, 2004b; Kuba, Yamada, Fukui, & Ohmori, 2005; Kuba, Adachi, & Ohmori, 2014), which were not identified by the mass spectrometry in this study.

NL is known to be highly metabolic. NL neurons generate high rates of action potentials, both in conditions of quiet and of acoustic stimulation (Born, Durham, & Rubel, 1991). Consistently, NL neurons contain a high density of mitochondria throughout their dendrites (Deitch & Rubel, 1989). Functionally, NL dendrites display high levels of energy consumption indicated by a high level of cytochrome oxidase and glucose uptake as measured by 2-deoxyglucose method (Dezso, Schwarz, & Schwarz, 1993; Heil & Scheich, 1986; Lippe, Steward, &
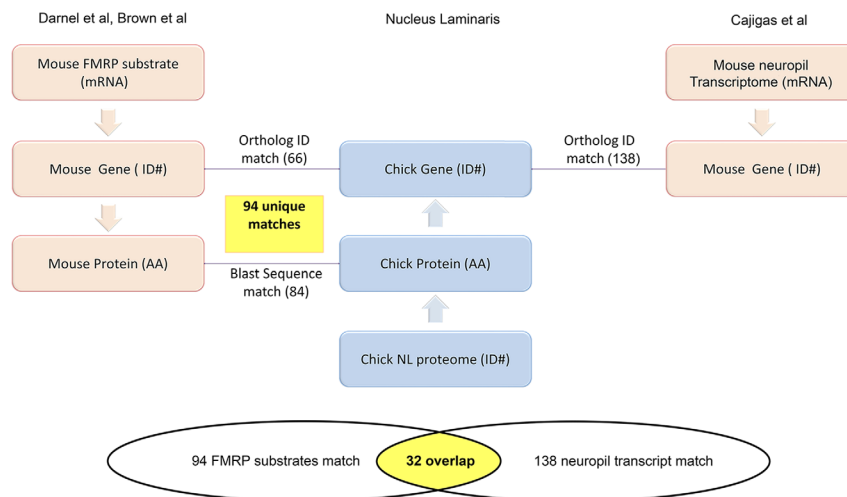
FIGURE 3 Schematic chart flow showing the approach used for identifying 94 unique proteins as candidate targets of FMRP in NL. We first combined the predicted mRNA targets of FMRP in the mouse brain from two studies (Brown et al., 2001; Darnell et al., 2011). We then created two databases with corresponding gene (ID#) and protein sequences (AA) using NCBI, ENSEMBL, BIOMART, and DAVID programs. Similarly, we generated two databases for protein sequence (AA) and corresponding gene (ID#) from the MS-identified proteins from the chicken NL. Finally, in order to find known equivalent FMRP from mice in our chicken NL proteome data, we employed the following strategy: find annotated orthologs (top line) or identify protein sequence matches (bottom line) by BLASTP. In total, 66 ortholog ID and 84 BLAST sequence matches were found, which together generate 94 unique matches. We also performed a comparison with a list of transcripts found in hippocampal neuropil (Cajigas et al., 2012). Of the 657 NL proteins, 138 targets match this list. Among the 138 matches, 32 candidates overlap with the 94 FMRP target candidates, presenting a selective list of proteins with a high likelihood of local translation in NL dendrites [Color figure can be viewed at wileyonlinelibrary.com]

TABLE 3 A list of 94 FMRP candidate substrates

GeneID	Symbol (alias)	Description	F	S	SC	BR	NCBI Reference
395373	ACLY	ATP citrate lyase	m	c	29	3	NP_001025711
374009	ACO2	aconitase 2, mitochondrial	m	m	246	4	NP_989519
396526	ACTB	actin, beta	c	c	286	3	NP_990849
423298	ACTC1	actin, alpha, cardiac muscle 1	c	c	213	3	NP_001072949
415296	ACTG1	Actin, gamma 1, cytoplasmic type 5	c	c	418	4	NP_001007825
422882	ADD1	adducin 1 (alpha)	c	c	17	2	NP_001073198
395492	ALDOC	aldolase C, fructose-bisphosphate	m	c	229	4	NP_001193425
420761	AMPH	amphiphysin	v	v	27	4	NP_001004398
423102	AP2A2	adaptor-related protein complex 2, alpha 2 subunit	v	p	20	2	NP_001012914
417525	AP2B1	adaptor-related protein complex 2, beta 1 subunit	v	p	21	3	XP_415772
420398	ARF1	ADP-ribosylation factor 1	v	v	25	2	NP_001006352
769725	ARF4	ADP-ribosylation factor 4	v	c	30	3	XP_001232784
396530	ATP1A1	ATPase, Na+/K+ transporting, alpha 1 polypeptide	t	p	294	4	NP_990852
396468	ATP1A2	ATPase, Na+/K+ transporting, alpha 2 polypeptide	t	p	607	4	NP_990807
396467	ATP1A3	ATPase, Na+/K+ transporting, alpha 3 polypeptide	t	v	773	4	NP_990806
396529	ATP1B1	ATPase, Na+/K+ transporting, beta 1 polypeptide	t	p	149	4	NP_990851
396446	ATP2A2 (SERCA2)	ATPase, Ca++ transporting, cardiac muscle, slow twitch 2; sarcoplasmic/endoplasmic reticulum calcium ATPase 2	t	v	8	2	XP_003642224
415958	ATP2B2	ATPase, Ca++ transporting, plasma membrane 2	t	p	43	4	XP_001231642
374159	ATP5A1	ATP synthase, H+ transporting, mitochondrial F1 complex, alpha subunit 1, cardiac muscle	t	p	370	4	NP_989617
431564	ATP5A1W	ATP synthase subunit alpha	t	m	349	4	XP_429118
426673	ATP5B	ATP synthase subunit beta, mitochondrial	t	m	366	4	NP_001026562
395497	ATP6V1B2 (VATB)	ATPase, H+ transporting, V-type proton ATPase subunit B	t	v	56	4	XP_424534
425976	BCAN	brevican	g	e	15	2	XP_423655
395855	CALM	calmodulin	s	c	125	4	NP_990336
417837	CAND1	cullin-associated and neddylation-dissociated 1	p	c	6	1	XP_416078
396248	CKB	creatine kinase, brain	m	m	628	4	NP_990641
395272	CLTC (CHC)	clathrin heavy chain 1	v	p	204	4	NP_001073586
416765	CLTCL1	clathrin, heavy chain-like 1	v	p	33	1	XP_415060
395921	CNP	2',3'-cyclic nucleotide 3' phosphodiesterase	g	p	639	4	NP_990381
427286	CPLX1	complexin 1	v	v	20	2	XP_424869
395156	CRMP1 (CRMP1B)	collapsin response mediator protein 1	g	c	66	4	NP_989826
417217	DNM1	dynamin 1	v	p	14	1	XP_415501
395155	DPYSL2 (CRMP2A)	dihydropyrimidinase-like 2, collapsin response mediator protein-2A	g	c	169	4	NP_989825
423461	DYNC1H1	dynein, cytoplasmic 1, heavy chain 1	v	c	57	3	XP_421371
373963	EEF1A1	eukaryotic translation elongation factor 1 alpha 1	tx	c	143	4	NP_989488
419244	EEF1A2	eukaryotic translation elongation factor 1 alpha 2	tx	c	98	4	NP_001027570

(Continues)

TABLE 3 (Continued)

GeneID	Symbol (alias)	Description	F	S	SC	BR	NCBI Reference
396325	EEF2	eukaryotic translation elongation factor 2	tx	c	80	4	NP_990699
419117	EPB41L1	erythrocyte membrane protein band 4.1-like 1	c	p	10	2	XP_417304
396061	FASN	fatty acid synthase, thioesterase	m	c	12	2	NP_990486
416485	FSCN1	fascin	c	c	172	4	NP_001171603
396489	GLUL	glutamine synthetase	m	m	247	4	NP_990824
419402	GNB1	guanine nucleotide binding protein (G protein), beta polypeptide 1	s	c	86	4	NP_001012853
424974	GNB4	guanine nucleotide binding protein (G protein), beta polypeptide 4	s	c	47	3	XP_003641822
373889	HK1	hexokinase 1	m	m	89	4	NP_989432
423463	HSP90AA1	heat shock protein HSP 90-alpha	p	c	333	4	NP_001103255
396188	HSP90AB1 (HSPCB)	heat shock cognate protein HSP 90-beta	p	c	23	1	NP_996842
408046	KIF5C	kinesin family member 5C	r	c	9	1	XP_422155
100857214	LOC100857214	tubulin alpha-4A chain-like	c	c	47	1	XP_003641691
100857247	LOC100857247	tubulin alpha-5 chain-like	c	c	254	4	XP_003641692
100857345	LOC100857345	V-type proton ATPase subunit d 1-like	t	v/p	3	1	XP_414041
100857582	LOC100857582	ubiquitin-like modifier-activating enzyme 1-like	p	c	2	1	XP_003643588
100858165	LOC100858165	V-type proton ATPase subunit d 1-like	t	v/p	3	1	XP_003643353
425049	LOC425049	tubulin alpha-3 chain-like	c	c	147	3	XP_422851
768337	LOC768337	tubulin beta-2 chain-like	c	c	187	2	XP_001231210
415588	MAP1A	microtubule-associated protein 1A	c	c	54	4	XP_003641886
396174	MAP1B	microtubule-associated protein 1B	c	c	5	1	XP_001231729
396097	MAP4	microtubule-associated protein 4	c	c	7	1	XP_418480
373953	MAPK1	mitogen-activated protein kinase 1	s	c	6	1	NP_989481
396217	MBP	myelin basic protein	s	p	726	4	NP_990611
396465	MYH10	myosin, heavy chain 10, non-muscle	c	c	8	1	NP_990805
428253	NCAM1	neural cell adhesion molecule 1	g	p	20	2	NP_001122300
768618	NDRG4	NDRG family member 4	s	c	9	2	XP_001231665
419972	NSF	N-ethylmaleimide-sensitive factor, vesicle-fusing ATPase	v	v	23	3	NP_001019627
426429	OGDH	2-oxoglutarate dehydrogenase, mitochondrial	m	m	58	4	NP_001026553
396214	PLP1	myelin proteolipid protein	g	p	231	4	NP_990608
395602	PSAP	prosaposin	m	v	2	1	NP_990142
374204	QKI	QKI, KH domain containing, RNA binding; protein quaking	s	p	13	2	NP_989641
395869	RHOC	ras homolog gene family, member C	s	c	29	3	NP_001025020
378791	RTN1	reticulon 1	g	v	13	3	NP_001001466
378790	RTN4 (NOGO)	reticulon 4	g	v	74	4	XP_003640941
416778	SEPT5	septin 5	g	c	36	4	NP_001025825
422954	SFXN5	sideroflexin 5	t	m	9	2	XP_420891

(Continues)

TABLE 3 (Continued)

GeneID	Symbol (alias)	Description	F	S	SC	BR	NCBI Reference
422971	SLC17A6 (VGLUT2)	solute carrier family 17 (sodium-dependent inorganic phosphate cotransporter), member 6; vesicular glutamate transporter 2	t	p	8	1	NP_001161855
423156	SLC1A2	solute carrier family 1 (glial high affinity glutamate transporter), member 2; excitatory amino acid transporter 2	t	p	80	4	NP_001012917
422649	SLC4A4	solute carrier family 4, sodium bicarbonate cotransporter, member 4	t	p	27	4	XP_420603
396444	SNAP25	synaptosomal-associated protein, 25kDa	v	v	6	1	NP_990789
428635	SNAP91	clathrin coat assembly protein AP180, synaptosomal-associated protein 91	v	p	13	2	NP_001012969
374234	SPTAN1 (SPECA)	spectrin alpha chain, non-erythrocytic 1	c	c	135	4	NP_001036003
421216	SPTBN1	spectrin beta chain, non-erythrocytic 1	c	c	137	4	NP_001186354
404293	STXBP1	syntaxin binding protein 1, Unc18–1	v	v	67	4	NP_996859
418015	SYNGR1	synaptogyrin 1	v	v	11	3	NP_001239207
418498	SYNJ1	synaptojanin 1	v	v	7	1	XP_416706
420800	TPPP	tubulin polymerization promoting protein	c	c	50	4	XP_418894
421169	TUBA3E	tubulin, alpha 3e	c	c	44	1	XP_419249
396254	TUBB	tubulin beta-7 chain	c	c	393	4	NP_990646
420883	TUBB2B (TUBB2)	tubulin beta-2 chain	c	c	331	4	NP_001004400
417255	TUBB2C (TUBB4)	tubulin, beta 2C; tubulin beta-3 chain	c	c	354	4	NP_001074329
431043	TUBB3	tubulin, beta 3 class III; tubulin beta-4 chain	c	c	303	4	NP_001026769
421037	TUBB6	tubulin, beta 6 class V; tubulin beta-5 chain	c	c	118	2	NP_001026183
416013	UQCRC1	ubiquinol-cytochrome c reductase core protein I	m	m	120	4	XP_414356
418290	USP5	ubiquitin specific peptidase 5 (isopeptidase T)	p	c	4	2	XP_003640490
418273	VAMP1	vesicle-associated membrane protein 1 (synaptobrevin 1)	v	v	21	3	NP_001034575
419368	VAMP3	vesicle-associated membrane protein 3 (cellubrevin)	v	v	24	3	NP_001034578
427820	YWHAG	14–3-3 protein gamma, tyrosine 3-monooxygenase/tryptophan 5-monooxygenase activation protein, gamma polypeptide	s	c	164	4	NP_001026648

Entrez gene identification number, official gene symbol and description are provided. Also provided are functional categorization (F), subcellular localization (S), the total number of spectral counts (SC) matching the protein and the number of biological replicates (BR) in which protein was identified (n = 4).

F – Functional categorization: c (cytoskeleton), g (cell growth), m (metabolism), p (protein modification), r (RNA transport), s (signaling), tx (translation), v (vesicle transport), t (ion/amine transport)

S – Subcellular categorization: c (cytosol), e (extracellular), m (mitochondrion), p (plasma membrane), v (vesicle)

Rubel, 1980). Using DAVID software (Huang da et al., 2008), we obtained corresponding gene IDs for the proteins identified from NL and BS. We looked for enriched pathways represented by the gene list compared to what would be expected from the *Gallus gallus* genome. Enrichment score of >1.3 is considered meaningful (Huang da et al., 2008). Among the top ten enriched pathways in the BS and NL samples, mitochondrial, metabolic and translation pathways were on the top in both sets of samples (Table 2), indicating that the protein identification of NL in this study reflects this prominent feature of high activity in NL.

3.2 | Comparative analyses identified 94 putative FMRP targets in NL

We were interested in determining which of the proteins identified were most likely to be translated locally in dendrites. In particular, we were interested in those proteins that may be products of mRNAs regulated by FMRP. We obtained a combined list of FMRP targets previously identified in mouse brains (Brown et al., 2001; Darnell et al., 2011). To allow comparative analyses between different species (mouse vs. chicken) and between RNA and amino acid sequence, we

TABLE 4 Enriched pathways of the 94 putative FMRP targets revealed by DAVID analysis

	FMRP substrate from NL	
	Cluster	Enrichment Score
1	Ribonucleotide Binding	6.66
2	GTPase/microtubule	3.47
3	ATPase/transmembrane transport	3.46
4	Neuronal projection	2.89
5	Methylation	2.67

Gene ontology analysis of these 94 select proteins suggests a role in ribonucleotide binding, transmembrane transport and cellular growth, pathways needed for structural changes.

first created databases for each list with corresponding RNA sequence, protein sequence, gene ID, and gene name using a combination of DAVID and Ensembl Bio-mart software (Figure 3). We performed comparative analyses first at the gene level by finding orthologous matches based on the aforementioned curated database of Gene IDs, and then by BLAST analysis to manually identify additional orthologs by sequence homology. In total, we found a unique list of 94 proteins that are products of putative FMRP targets (Table 3). Consistent with a recent study that described the characteristics of top FMRP binding transcripts as having >18 RNA WGGA or ACUK sequences (Ascano et al., 2012), all 94 putative FMRP candidates have these sequences and the majority of them (88 out of 94 candidates; 94%) have >18 copies of such sequences.

We performed DAVID analysis on the identified 94 proteins as putative FMRP targets (Table 4). In contrast to the previous analysis on all identified NL proteins, which revealed enrichment of pathways involved in metabolism, FMRP putative targets were enriched in pathways involved in cellular growth and transport (ribonucleotide binding, GTPases, ATPases, microtubules and neuronal projection) and transmembrane transport.

Further categorizing by subcellular localization (Figure 4b), we found that the majority of these 94 proteins (72%) were localized to the cytosol (49%) and vesicles (19%), although a sizeable portion (21%) were localized to the plasma membrane. Categorization by function (Figure 4a) reveals that the largest group (34% of proteins) was involved in cytoskeleton and cell growth, consistent with potential involvement of FMRP in regulating structural changes. The next most highly represented groups were those involved in intracellular trafficking (20%), useful in delivery of proteins needed to effect immediate changes, and those involved in transport across membranes (17%) including glutamate transporters.

3.3 | Comparative analyses identified 32 putative FMRP targets that maybe locally translated

Another group had previously published a list of transcripts found in hippocampal neuropil to determine locally translated proteins (Cajigas et al., 2012). We performed a comparison with this list and found that of the 657 NL proteins, 138 match this list (Figure 3). Of the 94 FMRP target candidates, 32 also match this list, which is a unique and selective list of proteins with a high likelihood of local translation in NL dendrites (Table 5).

The NL samples contain not only the somata and dendrites of NL neurons but also incoming axons of NM neurons and glia. The tissue samples used to generate the list of locally translated proteins in hippocampus (Cajigas et al., 2012) also contain dendrites, axons, and glial cells. As expected, a number of proteins in the 32 protein list are known to be specific to glial cells including the myelin basic protein (MBP) and N-myc downstream regulated gene (NDRG) family member 4 or proteins primarily localized in presynaptic compartments such as SNAP25. Other proteins such as MAP1B are expressed in both post and presynaptic ends. To further narrow down the list of promising FMRP targets in NL dendrites, we next examined the subcellular localization of a number of selected proteins included in the 94-protein list, in particular those included in the short 32-protein list.

3.4 | Immunocytochemistry confirms the expression of selected protein candidates in NL and their dendritic localization

We chose to focus on cytosolic proteins whose translation does not require Golgi, as no Golgi apparatus has been detected in NL dendrites at the electron microscope level (Deitch & Rubel, 1984). Since the 94 putative FMRP targets are enriched in pathways that facilitate structural changes, we first examined the distribution of cytoskeletal elements and their associated proteins. The NL dendrites were visualized by a neuronal somatodendritic marker, the microtubule associated protein 2 (MAP2). We used two antibodies for MAP2, raised in different hosts (rabbit and mouse), which show complete overlap of strong dendritic staining as well as weaker somatic staining (Figure 5a). The distribution of another microtubule associated protein, MAP1B, is illustrated in Figure 5b. Interestingly, the intensity of somatic MAP1B immunoreactivity varies among NL neurons. In the neuropil regions, prominent MAP1B immunoreactivity was largely located outside of MAP2-stained NL dendrites. The distribution of the beta tubulin class III (TUBB3) was examined using TUJ1 immunoreactivity, a specific marker for this type of tubulin. TUJ1 staining was strong in both cell bodies and the primary dendrites. Diffuse staining also overlapped with MAP2-stained dendrites further from the cell bodies (Figure 5c). Fluorescent conjugated phalloidin was used to visualize F-actin. As expected, F-actin stain displayed a peri-membrane pattern, surrounding MAP2-stained cell bodies and dendritic structure (Figure 5d).

We next examined the three eukaryotic elongation factor proteins (eEF) that were included in the 32-protein list, eEF1a1, eEF1a2, and eEF2. Using an antibody that specifically recognizes the phosphorylated form of eEF (p-eEF2), we identified the distribution of p-eEF2 in NL cell bodies as well as MAP2-stained dendrites at varied levels (Figure 6a). In contrast, we only observed a somatic distribution of eEF1a in NL using an antibody recognizing both eEF1a1 and eEF1a2 (Figure 6b).
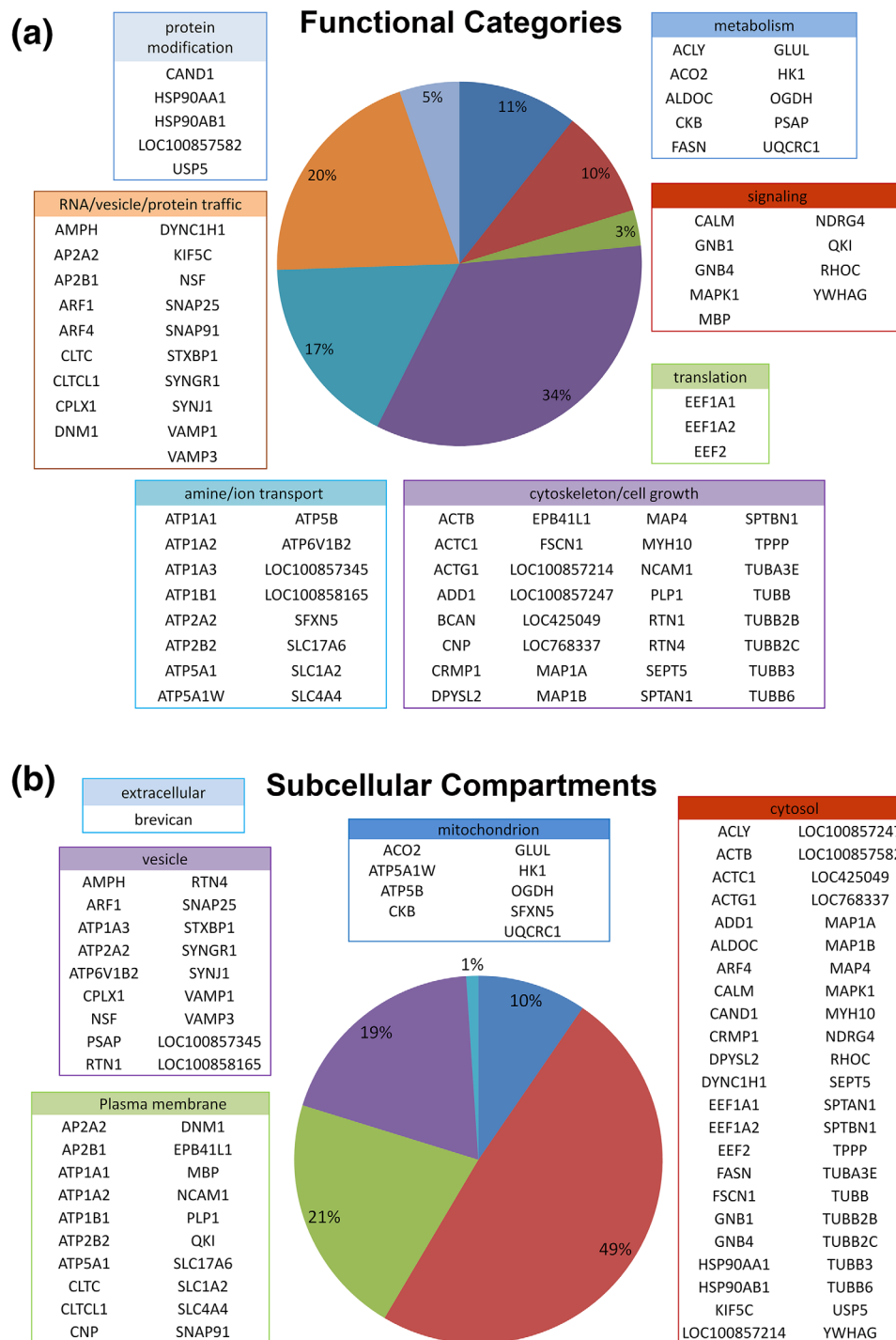
(a) Functional Categories

protein modification
CAND1
HSP90AA1
HSP90AB1
LOC100857582
USP5

metabolism

ACLY	GLUL
ACO2	HK1
ALDOC	OGDH
CKB	PSAP
FASN	UQCRC1

RNA/vesicle/protein traffic

AMPH	DYNC1H1
AP2A2	KIF5C
AP2B1	NSF
ARF1	SNAP25
ARF4	SNAP91
CLTC	STXBP1
CLTCL1	SYNGR1
CPLX1	SYNJ1
DNM1	VAMP1
	VAMP3

signaling

CALM	NDRG4
GNB1	QKI
GNB4	RHOC
MAPK1	YWHAG
MBP	

translation
EEF1A1
EEF1A2
EEF2

amine/ion transport

ATP1A1	ATP5B
ATP1A2	ATP6V1B2
ATP1A3	LOC100857345
ATP1B1	LOC100858165
ATP2A2	SFXN5
ATP2B2	SLC17A6
ATP5A1	SLC1A2
ATP5A1W	SLC4A4

cytoskeleton/cell growth

ACTB	EPB41L1	MAP4	SPTBN1
ACTC1	FSCN1	MYH10	TPPP
ACTG1	LOC100857214	NCAM1	TUBA3E
ADD1	LOC100857247	PLP1	TUBB
BCAN	LOC425049	RTN1	TUBB2B
CNP	LOC768337	RTN4	TUBB2C
CRMP1	MAP1A	SEPT5	TUBB3
DPYSL2	MAP1B	SPTAN1	TUBB6

(b) Subcellular Compartments

extracellular
brevican

vesicle

AMPH	RTN4
ARF1	SNAP25
ATP1A3	STXBP1
ATP2A2	SYNGR1
ATP6V1B2	SYNJ1
CPLX1	VAMP1
NSF	VAMP3
PSAP	LOC100857345
RTN1	LOC100858165

mitochondrion

ACO2	GLUL
ATP5A1W	HK1
ATP5B	OGDH
CKB	SFXN5
	UQCRC1

cytosol

ACLY	LOC100857247
ACTB	LOC100857582
ACTC1	LOC425049
ACTG1	LOC768337
ADD1	MAP1A
ALDOC	MAP1B
ARF4	MAP4
CALM	MAPK1
CAND1	MYH10
CRMP1	NDRG4
DPYSL2	RHOC
DYNC1H1	SEPT5
EEF1A1	SPTAN1
EEF1A2	SPTBN1
EEF2	TPPP
FASN	TUBA3E
FSCN1	TUBB
GNB1	TUBB2B
GNB4	TUBB2C
HSP90AA1	TUBB3
HSP90AB1	TUBB6
KIF5C	USP5
LOC100857214	YWHAG

Plasma membrane

AP2A2	DNM1
AP2B1	EPB41L1
ATP1A1	MBP
ATP1A2	NCAM1
ATP1B1	PLP1
ATP2B2	QKI
ATP5A1	SLC17A6
CLTC	SLC1A2
CLTCL1	SLC4A4
CNP	SNAP91

FIGURE 4 Characterization of 94 FMRP candidate targets. Using DAVID program, the proteins were subdivided by function (a) and subcellular compartments (b). The names of individual proteins are listed in specific category boxes with corresponding colors. A majority of the proteins are involved in cell growth 34%, intracellular trafficking 20% and transmembrane transport 17%. About half (49%) of the proteins are cytosolic proteins with the second half associated with plasma membrane, mitochondria, and vesicles. One protein was predicted to have an extracellular localization [Color figure can be viewed at wileyonlinelibrary.com]

Finally, we examined three proteins involved in signaling regulation. As an important mechanism for calcium regulation, SERCA2 immunoreactivity was detected in some MAP2-labeled NL dendrites in addition to expected somatic staining (Figure 7a). N-ethylmaleimide-sensitive factor (NSF) is a vesicle fusion protein. As expected (Serwin, 2012), NSF was strongly localized along perinuclear and cytoplasmic regions (Figure 7b). In addition, significant NSF immunoreactivity was detected in the NL neuropil regions. Ras homolog gene family member C (RhoC) is a small G-protein that can promote remodeling of actin cytoskeleton. Immunocytochemistry revealed a particularly high level of RhoC protein in NL dendrites (Figure 7c).

TABLE 5 Thirty-two of the 94 FMRP targets likely to be translated locally

Cell growth/cytoskeleton	
CRMP1	collapsin response mediator protein 1
MAP1B	microtubule-associated protein 1B
ACTG1	Actin, gamma 1
SPTBN1	spectrin, beta, non-erythrocytic 1
TUBB	tubulin, beta class I
TUBB2C	tubulin, beta 2C
TUBB2B	tubulin, beta 2B class IIb
TUBB3	tubulin, beta 3 class III
Transport of ions/amines (integral membrane proteins)	
ATP6V1B2 (VATB)	ATPase, H+ transporting, lysosomal 56/58kDa, V1 subunit B2
ATP2A2 (SERCA2)	ATPase, Ca++ transporting, cardiac muscle, slow twitch 2
ATP1B1	ATPase, Na+/K+ transporting, beta 1 polypeptide
ATP1A1	ATPase, Na+/K+ transporting, alpha 1 polypeptide
LOC100857345	V-type proton ATPase subunit d 1-like
LOC100858165	V-type proton ATPase subunit d 1-like
Metabolism	
HK1	hexokinase 1
ACO2	aconitase 2, mitochondrial
Protein Modification	
USP5	ubiquitin specific peptidase 5 (isopeptidase T)
Trafficking of RNA, proteins or vesicles	
KIF5C	kinesin family member 5C
DYNC1H1	dynein, cytoplasmic 1, heavy chain 1
DNM1	dynamin 1
ARF1	ADP-ribosylation factor 1
AMPH	amphiphysin
SNAP25	synaptosomal-associated protein, 25kDa
SYNJ1	synaptojanin 1
NSF	N-ethylmaleimide-sensitive factor
SNAP91	synaptosomal-associated protein, 91kDa homolog (mouse)
Signaling	
CALM	calmodulin 2 (phosphorylase kinase, delta)
MBP	myelin basic protein
NDRG4	N-myc downstream regulated gene family member 4
Translation	
EEF2	eukaryotic translation elongation factor 2
EEF1A1	eukaryotic translation elongation factor 1 alpha 1
EEF1A2	eukaryotic translation elongation factor 1 alpha 2
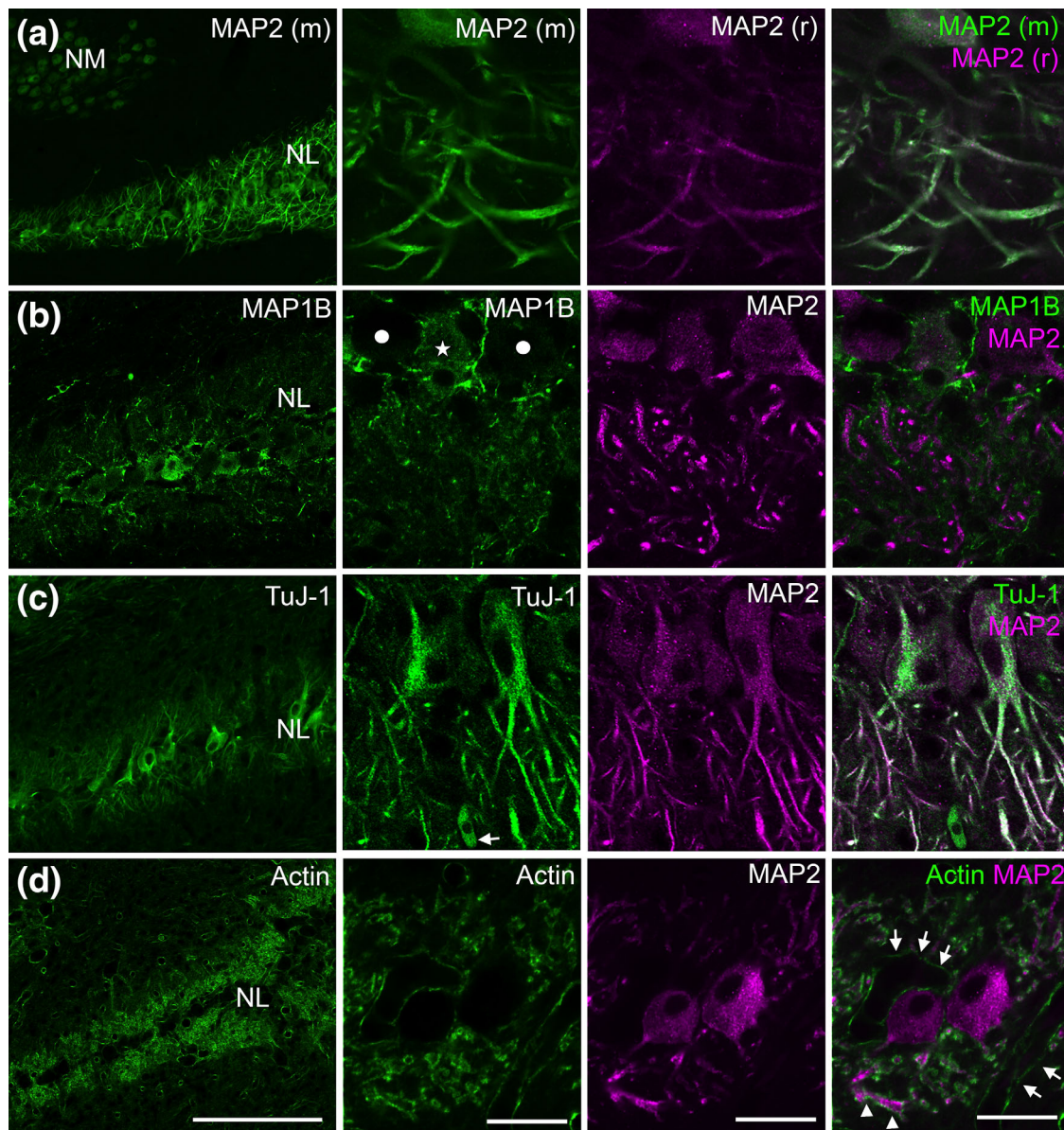
FIGURE 5 Subcellular distribution of cytoskeletal elements and their associated proteins in NL examined by immunocytochemistry. (a) Two antibodies for MAP2 raised in rabbit (r) or mouse (m) display identical dendritic labeling in NL. These two antibodies are subsequently used as dendritic markers for examining the localization of other protein candidates. (b) Double labeling of MAP1B and MAP2. Strong MAP1B immunoreactivity in NL neuropil regions does not overlap with MAP2-labeled dendrites. Detectable MAP1B immunoreactivity is found in some (white star) but no other NL cell bodies (solid white circles). (c) Double labeling of TuJ-1 and MAP2. TuJ-1 immunoreactivity is strong in the cell bodies and the primary portions of dendrites, and relatively weaker in the more distal dendritic branches. (d) Phalloidin stain visualizing the distribution of F-actin surrounding MAP2 labeled dendritic branches (arrowheads). Arrows point to phalloidin stain along blood vesicles. Abbreviations: NM, nucleus magnocellularis; NL, nucleus laminaris; TuJ-1, neuron-specific class III beta-tubulin; MAP2, microtubule-associated protein 2; MAP1B, microtubule-associated protein 1B. Scale bar = 100 μm (left column) and 20 μm (all other columns) [Color figure can be viewed at wileyonlinelibrary.com]

3.5 | RNA electrophoretic-mobility shift assay reveals FMRP interaction with RhoC RNA

RhoC is of particular interest as a potential FMRP target due to its function in signal transduction and cytoskeleton regulation, as well as its intense localization in NL dendrites. In order to validate the interaction of RhoC with FMRP, we performed RNA binding assays with recombinant chicken FMRP. Figure 8 shows specific interaction between FMRP and RhoC RNA. When biotin-labeled RhoC RNA probe was incubated with purified FMRP, we detected a shift on the probe indicating their interaction in vitro (lanes 1 and 2). The specificity of this interaction was demonstrated when unlabeled RhoC probe competed for FRMP binding in a dose dependent manner (lanes 3–6), which was not observed if RhoC probe was replaced with a non-specific RNA probe (lanes 7–10).
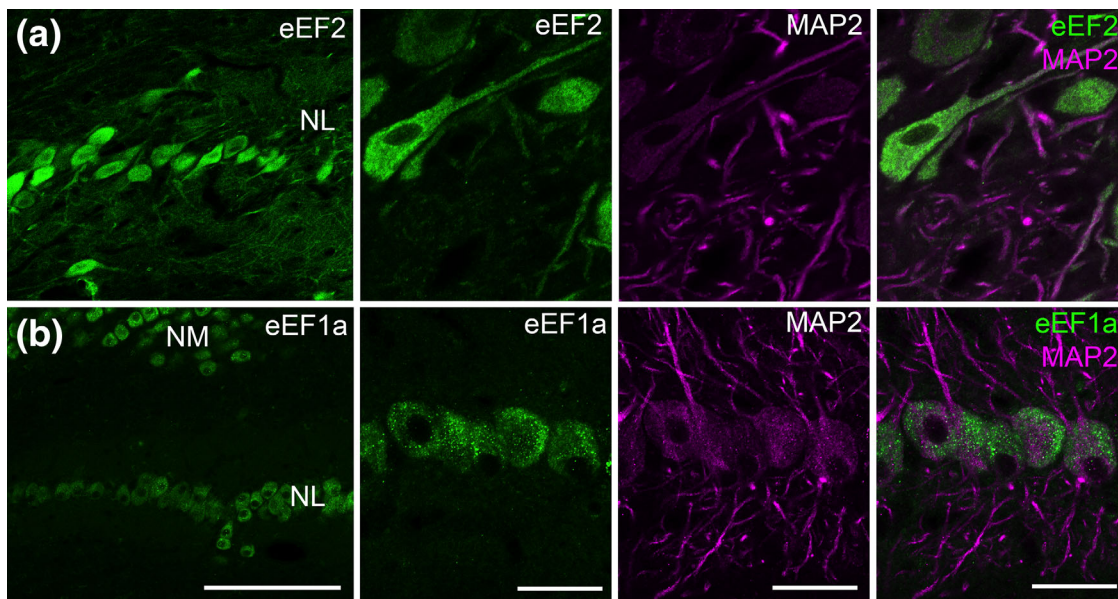
FIGURE 6 Subcellular distribution of elongation factors 1a and 2 in NL examined by immunocytochemistry. (a) Double labeling of phosphorylated eEF2 (p-eEF2) and MAP2, showing the distribution of eEF2 in both cell bodies and dendrites of NL neurons. Dendritic level of p-eEF2 varies between branches. (b) Double labeling of eEF1a and MAP2. Strong immunoreactivity for eEF1a was observed in NL cell bodies, while no detectable staining was found in NL neuropil regions containing dendrites. Abbreviations: NM, nucleus magnocellularis; NL, nucleus laminaris; MAP2, microtubule-associated protein 2; eEF1a, eukaryotic elongation factor 1a; eEF2, eukaryotic elongation factor 2. Scale bar = 100 μm (left column) and 20 μm (all other columns) [Color figure can be viewed at wileyonlinelibrary.com]

4 | DISCUSSION

NL is a critical structure for localizing the source of sound, necessary processing for acoustic scene analysis. Given its unique bipolar dendritic structure and highly dynamic structural properties of these dendrites (Sorensen & Rubel, 2006), NL is also a particularly useful model for studying the neuroplasticity of dendrites in response to afferent stimulation. In view of the growing acceptance for a critical role of local protein translation in dendritic neuroplasticity (Steward et al., 2014), the proteome of NL dendrites would be useful for determining local proteins that are being differentially translated during periods of dendritic remodeling. In this study, we present an initial proteomic analysis of NL with identification of 657 proteins, of which 94 are putative targets of FMRP, an mRNA-binding protein that regulates local protein translation in neural dendrites.

4.1 | Methodological consideration

Two limitations need to be taken into consideration before applying the data generated in this study into future studies. First, the 657 proteins identified for NL is a conservative list of all proteins expressed by NL neurons and these proteins may be biased towards soluble proteins. This bias may be attributed to several factors. One is the lack of sufficient tissue, given the small size of the nucleus, to perform subcellular fractionation to enrich for membrane proteins, which are usually low abundance proteins. It is also possible that laser capture of dehydrated tissues may hinder the extraction of lipophilic molecules. Lastly, the hydrophobicity of membrane proteins renders them less accessible for trypsin digestion given that their hydrophobic regions are not accessible. On the other hand, the list of NL proteins we provide is a consistent list of proteins sampled reproducibly in

multiple replicates. Due to the stochastic sampling of tandem mass spectrometry data using data dependent acquisition, the repeatability of peptides identified between technical replicates has been reported to range between 35% and 60% (Tabb et al., 2010). This variability is increased with greater complexity of the protein sample. We collected proteins from a single brainstem nucleus and we required each peptide to present in every technical replicate ($n = 3$) and at least two peptides per protein for identification. With these strict requirements, we have 96% overlap of NL samples with BS list. This suggests a conservative list of proteins but likely biased towards more abundant proteins.

Second, the comparative analyses were performed to identify the most promising protein candidates that may be involved in potential FMRP regulation of NL dendrites. These comparisons did not take into consideration of potential interspecies variation of FMRP signals and function (Kwan et al., 2012). As a result, our 94 and 32 protein lists likely contain both false positive and false negative candidates. In addition, we did not attempt to unambiguously validate any FMRP target in this study. Immunocytochemical and in vitro RNA binding experiments aimed to further narrow down the list of protein candidates. Dendritic localization and the ability of binding FMRP in vitro are necessary, although not sufficient, as a FMRP target in neuronal dendrites. Functional manipulations combined with co-immunoprecipitation analyses are required for validating each FMRP target in future studies.

4.2 | Proteins of interest

Many identified proteins in the 94-list are cytoskeletal elements (Actin and Tubulin) and their associated proteins (MAPs). Immunocytochemistry confirmed the dendritic localization of F-actin, beta 3 class III tubulins,
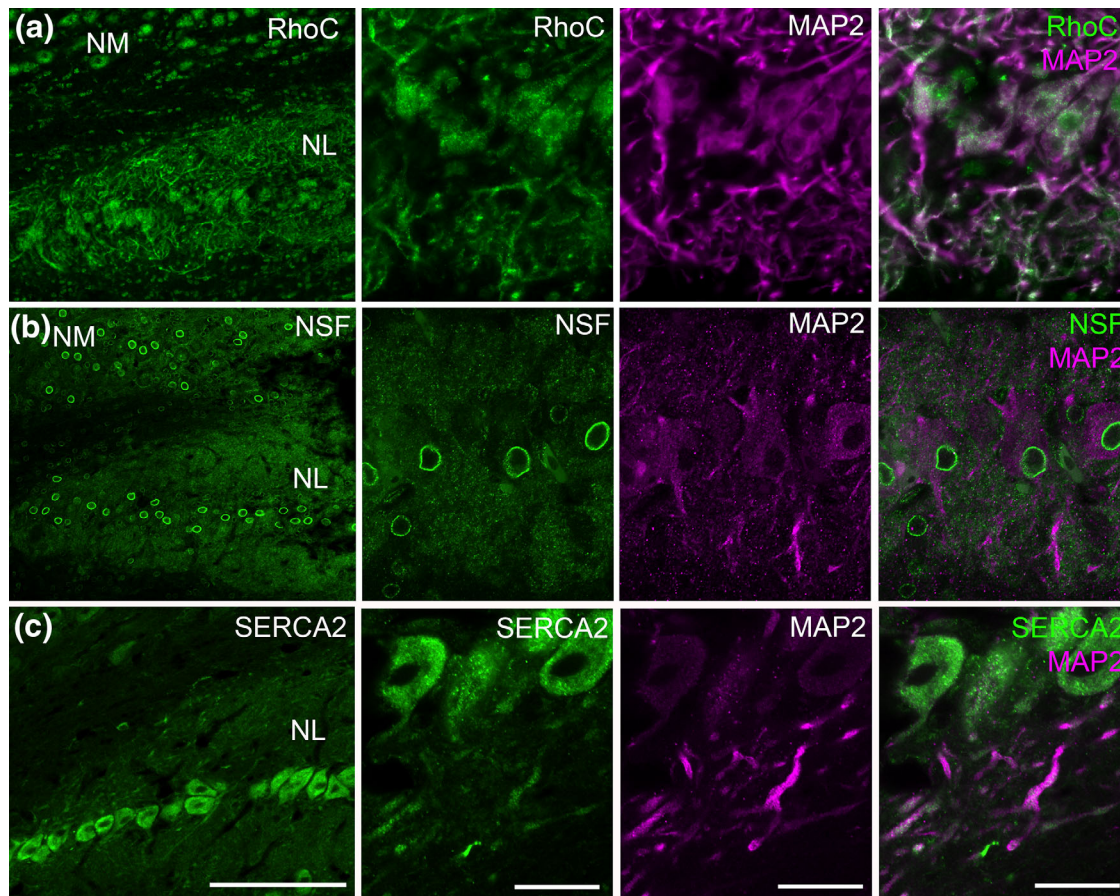
FIGURE 7 Subcellular distribution of NSF, SERCA2 and RhoC in NL examined by immunocytochemistry. (a) Double labeling of NSF and MAP2, showing localization of NSF in NL dendrites in addition to intense perinuclear staining. (b) Double labeling of SERCA2 and MAP2. In addition to the cell bodies, SERCA2 is also localized in NL dendrites. (c) Double labeling of RhoC and MAP2, showing an intense localization of RhoC overlapping with MAP2-labeled NL dendrites. Abbreviations: NM, nucleus magnocellularis; NL, nucleus laminaris; MAP2, microtubule-associated protein 2; SERCA2, sarco/endoplasmic reticulum Ca^{2+} ATPase. Scale bar = 100 μm (left column) and 20 μm (all other columns) [Color figure can be viewed at wileyonlinelibrary.com]

and MAP2, suggesting that FMRP may regulate both actin and microtubule function in NL dendrites. Interestingly, MAP1B does not display significant dendritic localization, although it is detected in a subpopulation of NL cell bodies. Genes encoding MAP1B and MAP2 are both predicted to have strong associations with FMRP (ranking 5 and 62 among 842 FMRP-associated genes, Darnell et al., 2011). Extensive evidence has confirmed the colocalization of FMRP with MAP1B mRNA in both dendrites and axons (Antar, Dictenberg, Plociniak, Afroz, & Bassel, 2005; Antar, Li, Zhang, Carroll, & Bassel, 2006). MAP1B protein level is elevated in hippocampus of Fmr1 knockout mice although the subcellular localization of the elevated MAP1B is unknown (Lu et al., 2004a). In particular, it has been shown that FMRP regulates MAP1B translation and controls microtubule stability in vertebrate neurons in vivo (Lu et al., 2004a; Zalfa et al., 2003). Lack of significant amount of MAP1B protein in NL dendrites may indicate the FMRP-MAP1B mRNA is a less prominent pathway in regulating microtubule in NL dendrites, as compared to potential FMRP regulation of MAP2 signaling. We did observe MAP1B positive fibers in the NL neuropil layer, presumably on incoming NM axons. Direct targeting of FMRP to MAP1B has been observed in axons and to

regulate axon elongation (Wang et al., 2015). These observations further support the possibility that FMRP signaling is cell type specific.

In our analysis, we identified three elongation factors as FMRP targets, two isoforms of eEF1a and eEF2. Furthermore, we visualized dendritic localization of eEF2 but not of eEF1a in NL neurons, suggesting that FMRP may affect dendritic protein synthesis by modulating a subset of translational regulatory machinery. Although a direct link between FMRP and eEF1a and eEF2 mRNAs has not been demonstrated, both of these two elongation factors have been associated with potential roles in cellular growth/proliferation and signal transduction (Lin, Yakymovych, Jia, Yakymovych, & Souchelnytskyi, 2010; Morrissey et al., 2015) as well as synaptic regulation (Becker, Kuhse, & Kirsch, 2013; Mateyak & Kinzy, 2010; Rosenblum, Meiri, & Dudai, 1993). In particular, eEF2 has recently been considered as a biochemical sensor that couples neuronal transmission to spine plasticity, a major proposed function of FMRP signaling (Verpelli et al., 2010).

This study also identified a number of dendritic localizing proteins that are predicted to be FMRP targets (Brown et al., 2001; Darnell et al., 2011), but their interaction with FMRP has yet to be validated.
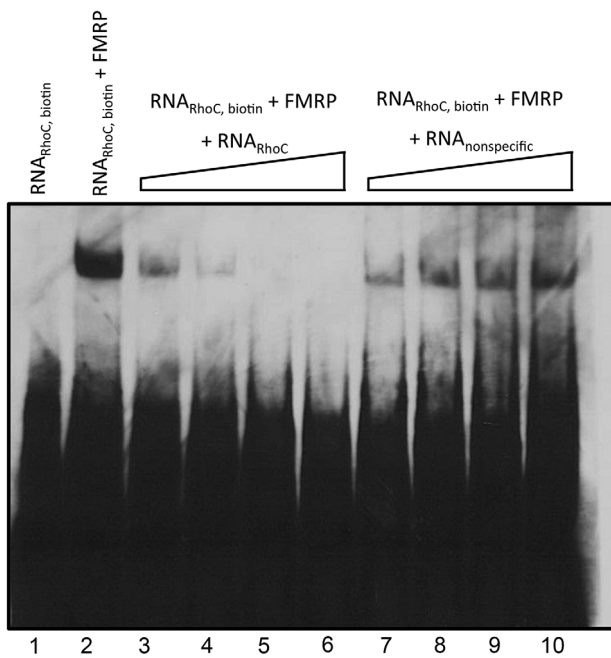
FIGURE 8 FMRP binds specifically to RhoC RNA. RNA electrophoretic mobility shift assay was performed to verify direct interaction between RhoC RNA and recombinant FMRP as described in the Material and Methods. Lane 1, biotin labeled RhoC RNA alone. Lane 2, biotin labeled RhoC RNA plus FMRP. Lanes 3–6, biotin labeled RhoC RNA plus FMRP with increasing concentrations of unlabeled RhoC RNA. Lanes 7–10 biotin labeled RhoC RNA plus FMRP with increasing concentrations of non-specific competitor RNA. Both unlabeled RNA competitors are at $10\times$, $20\times$, $40\times$, $100\times$ fold excess of the biotin labeled RhoC RNA

SERCA2 is an intracellular calcium ATPase pump located in the sarcoplasmic reticulum. Although a possible link between SERCA2 and FMRP has not been reported, recent studies demonstrated that FMRP regulates depolarization-induced calcium signal in critical periods of drosophila brain development (Doll & Broadie, 2016). Interestingly, another calcium regulator, the plasmid membrane calcium ATPases type 2 (PMCA2) is also a predicted FMRP target with highest binding affinity with FMRP (ranking 10 among 842; [Darnell et al., 2011]). Importantly, PMCA2 is intensely localized in NL dendrites and its protein levels rapidly change in response to afferent deprivation in shortening NL dendrites (Wang et al., 2009).

Another newly identified protein, as a potential FMRP target in the dendritic region of NL is NSF. NSF is a SNARE protein, reported to be in postsynaptic SNARES involved in synapses and synaptic transmission. NSF binding to AMPA receptor GluA2 intracellular domain has been shown to regulate the plasma membrane insertion of GluA2 (Araki, Lin, & Huganir, 2010). Recent reports suggest an indirect role of NSF in synaptic plasticity by way of regulating glutamate receptor plasma membrane expression (Huganir & Nicoll, 2013).

RhoC is a GTPase localized near cell membranes and is thought to share overlapping roles with RhoA, which is better characterized and shown to be important in neuronal migration through effects on actin and microtubule cytoskeleton (Stankiewicz & Linseman, 2014). There is also evidence that inactivation of RhoA results in increased dendrite

arbor growth rate (Govek, Newey, & Van Aelst, 2005). In addition, in vitro studies of neonatal neurons indicate that reduction of RhoA and RhoC leads to the impaired dendritic growth (Calvet, Doherty, & Prochiantz, 1998), which suggests that RhoC may be required for normal dendritic development. The intense localization of RhoC in NL dendrites may imply an important role of RhoC in NL dendritic dynamics, likely through effects on actin polymerization. It is possible that FMRP locally regulates the translation of targets such as RhoC, within NL dendrites, to control dendritic structural changes in response to neuronal activity. In support of this notion, we verified the FMRP interaction in vitro with a partial RhoC RNA containing several predicted FMRP binding sites (Anderson et al., 2016). This result indicates that the comparative analysis performed in this study indeed generates promising FMRP target candidates and has great potential for identifying novel FMRP signaling pathways. It would be interesting, as future studies, to explore the interaction of the identified putative FMRP targets with FMRP in NL dendrites in vivo in response to auditory stimulation or unilateral auditory deafferentation.

5 | CONCLUSION

In summary, the data generated in this study provides a first proteomic analysis of NL. Comparison analyses generated a list of 94 proteins as potential FMRP targets. As initiated in the current study, subcellular localization of individual protein and its mRNA as well as their interaction with FMRP need to be confirmed and characterized using multiple approaches, including immunocytochemistry, in situ hybridization, immunoprecipitation, as well as loss-of-function studies.

DATA ACCESSIBILITY

The Full lists of MS-identified proteins will be deposited onto the Biolucida Cloud server maintained by MBF Biosciences upon the acceptance of the manuscript.

REFERENCES

Anderson, B. R., Chopra, P., Suhl, J. A., Warren, S. T., & Bassel, G. J. (2016). Identification of consensus binding sites clarifies FMRP binding determinants. *Nucleic Acids Research*, 44, 6649–6659.

Antar, L. N., Dictenberg, J. B., Plociniak, M., Afroz, R., & Bassel, G. J. (2005). Localization of FMRP-associated mRNA granules and requirement of microtubules for activity-dependent trafficking in hippocampal neurons. *Genes, Brain and Behavior*, 4, 350–359.

Antar, L. N., Li, C., Zhang, H., Carroll, R. C., & Bassel, G. J. (2006). Local functions for FMRP in axon growth cone motility and activity-dependent regulation of filopodia and spine synapses. *Molecular and Cellular Neuroscience*, 32, 37–48.

Araki, Y., Lin, D. T., & Hunganir, R. L. (2010). Plasma membrane insertion of the AMPA receptor GluA2 subunit is regulated by NSF binding and Q/R editing of the ion pore. *Proceedings of the National Academy of Sciences of the United States of America*, 107, 11080–11085.

Ashida, G., & Carr, C. E. (2011). Sound localization: Jeffress and beyond. *Current Opinion in Neurobiology*, 21, 745–751.

Ascano, M. J., Mukherjee, N., Bandaru, P., Miller, J. B., Nusbaum, J. D., Corcoran, D. L., . . . Tuschl, T. (2012). FMRP targets distinct mRNA sequence elements to regulate protein expression. *Nature*, 492, 382–386.

Becker, M., Kuhse, J., & Kirsch, J. (2013). Effects of two elongation factor 1A isoforms on the formation of gephyrin clusters at inhibitory synapses in hippocampal neurons. *Histochemistry and Cell Biology*, 140, 603–609.

Benes, F. M., Parks, T. N., & Rubel, E. W. (1977). Rapid dendritic atrophy following deafferentation: An EM morphometric analysis. *Brain Research*, 122, 1–13.

Born, D. E., Durham, D., & Rubel, E. W. (1991). Afferent influences on brainstem auditory nuclei of the chick: Nucleus magnocellularis neuronal activity following cochlea removal. *Brain Research*, 557, 37–47.

Boström, P., Anderson, L., Rutberg, M., Perman, J., Lidberg, U., Johansson, B. R., . . . Olofsson, S. O. (2007). SNARE proteins mediate fusion between cytosolic lipid droplets and are implicated in insulin sensitivity. *Nature Cell Biology*, 9, 1286–1293.

Brown, V., Jin, P., Ceman, S., Darnell, J. C., O'Donnell, W. T., Tenenbaum, S. A., . . . Warren, S. T. (2001). Microarray identification of FMRP-associated brain mRNAs and altered mRNA translational profiles in fragile X syndrome. *Cell*, 107, 477–487.

Cajigas, I. J., Tushev, T., Will, T. J., tom Dieck, S., Fuerst, N., & Schuman, E. M. (2012). The local transcriptome in the synaptic neuropil revealed by deep sequencing and high-resolution imaging. *Neuron*, 453, 453–466.

Calvet, S., Doherty, P., & Prochiantz, A. (1998). Identification of a signaling pathway activated specifically in the somatodendritic compartment by a heparan sulfate that regulates dendrite growth. *Journal of Neuroscience*, 18, 9751–9765.

Chami, M., Gozuacik, D., Lagorce, D., Brini, M., Falson, P., Peaucellier, G., . . . Paterlini-Bréchot, P. (2001). SERCA1 truncated proteins unable to pump calcium reduce the endoplasmic reticulum calcium concentration and induce apoptosis. *Journal of Cell Biology*, 153, 1301–1314.

Chen, L., & Toth, M. (2001). Fragile X mice develop sensory hyperreactivity to auditory stimuli. *Neuroscience*, 103, 1043–1050.

Darnell, J. C., Van Driesche, S. J., Zhang, C., Hung, K. Y., Mele, A., Fraser, C. E., . . . Darnell, R. B. (2011). FMRP stalls ribosomal translocation on mRNAs linked to synaptic function and autism. *Cell*, 146, 247–261.

Deitch, J. S., & Rubel, E. W. (1984). Afferent influences on brain stem auditory nuclei of the chicken: Time course and specificity of dendritic atrophy following deafferentation. *Journal of Comparative Neurology*, 229, 66–79.

Deitch, J. S., & Rubel, E. W. (1989). Changes in neuronal cell bodies in *N. laminaris* during deafferentation-induced dendritic atrophy. *Journal of Comparative Neurology*, 281, 259–268.

Dezso, A., Schwarz, D. W., & Schwarz, I. E. (1993). A survey of auditory brainstem nuclei in the chicken (Gallus domesticus) with cytochrome oxidase histochemistry. *Journal of Otolaryngology*, 22, 385–390.

DiTella, M. C., Feiguin, F., Carri, N., Kosik, K. S., & Cáceres, A. (1996). MAP-1B/TAU functional redundancy during laminin-enhanced axonal growth. *Journal of Cell Science*, 109, 467–477.

Doll, C. A., & Broadie, K. (2016). Neuron class-specific requirements for Fragile X Mental Retardation Protein in critical period development of calcium signaling in learning and memory circuitry. *Neurobiology of Disease*, 89, 76–87.

Eng, J. K., McCormack, A. L., & Yates, J. R. (1994). An approach to correlate tandem mass spectral data of peptides with amino acid sequences in a protein database. *Journal of the American Society for Mass Spectrometry*, 5, 976–989.

Eriksson, M., Samuelsson, H., Björklund, S., Tortosa, E., Avila, J., Samuelsson, E. B., . . . Sundström, E. (2010). MAP1B binds to the NMDA receptor subunit NR3A and affects NR3A protein concentrations. *Neuroscience Letters*, 471(1), 33–37.

Franzen, R., Tanner, S. L., Dashiell, S. M., Rottkamp, C. A., Hammer, J. A., & Quarles, R. H. (2001). Microtubule-associated protein 1B: A neuronal binding partner for myelin-associated glycoprotein. *Journal of Cell Biology*, 155, 893–898.

Galvez, R., Gopal, A. R., & Greenough, W. T. (2003). Somatosensory cortical barrel dendritic abnormalities in a mouse model of the fragile X mental retardation syndrome. *Brain Research*, 971, 83–89.

Galvez, R., & Greenough, W. T. (2005). Sequence of abnormal dendritic spine development in primary somatosensory cortex of a mouse model of the fragile X mental retardation syndrome. *American Journal of Medical Genetics Part A*, 135, 155–160.

Govek, E. E., Newey, S. E., & Van Aelst, L. (2005). The role of the Rho GTPases in neuronal development. *Genes & Development*, 19, 1–49.

Grothe, B. (2000). The evolution of temporal processing in the medial superior olive, an auditory brainstem structure. *Progress in Neurobiology*, 61, 581–610.

Heil, P., & Scheich, H. (1986). Effects of unilateral and bilateral cochlea removal on 2-deoxyglucose patterns in the chick auditory system. *Journal of Comparative Neurology*, 252, 279–301.

Hinton, V. J., Brown, W. T., Wisniewski, K., & Rudelli, R. D. (1991). Analysis of neocortex in three males with the fragile X syndrome. *American Journal of Medical Genetics*, 41, 289–294.

Huang da, W., Sherman, B. T., Stephens, R., Baseler, M. W., Lane, H. C., & Lempicki, R. A. (2008). DAVID gene ID conversion tool. *Bioinformation*, 2, 428–430.

Huganir, R. L., & Nicoll, R. A. (2013). AMPARs and synaptic plasticity: The last 25 years. *Neuron*, 80, 704–717.

Impens, F., Van Damme, P., Demol, H., Van Damme, J., Vandekerckhove, J., & Gevaert, K. (2008). Mechanistic insight into taxol-induced cell death. *Oncogene*, 27, 4580–4591.

Irwin, S. A., Galvez, R., & Greenough, W. T. (2000). Dendritic spine structural anomalies in fragile-X mental retardation syndrome. *Cerebral Cortex*, 10, 1038–1044.

Joris, P., & Yin, T. C. (2007). A matter of time: Internal delays in binaural processing. *Trends in Neurosciences*, 30, 70–78.

Käll, L., Canterbury, J. D., Weston, J., Noble, W. S., & MacCoss, M. J. (2007). Semi-supervised learning for peptide identification from shotgun proteomics datasets. *Nature Methods*, 4, 923–925.

Kaur, K. J., & Ruben, L. (1994). Protein translation elongation factor-1 alpha from Trypanosoma brucei binds calmodulin. *Journal of Biological Chemistry*, 269, 23045–23050.

Kuba, H., Yamada, R., Fukui, I., & Ohmori, H. (2005). Tonotopic specialization of auditory coincidence detection in nucleus laminaris of the chick. *Journal of Neurosciences*, 25(8), 1924–1934.

Kuba, H. (2007). Cellular and molecular mechanisms of avian auditory coincidence detection. *Neuroscience Research*, 59, 370–376.

Kuba, H., Adachi, R., & Ohmori, H. (2014). Activity-dependent and activity-independent development of the axon initial segment. *Journal of Neuroscience*, 34(9), 3443–4353.

Kwan, K. Y., Lam, M. M., Johnson, M. B., Dube, U., Shim, S., Rašin, M. R., . . . Sestan, N. (2012). Species-dependent posttranscriptional

regulation of NOS1 by FMRP in the developing cerebral cortex. *Cell*, *149*(4), 899–911.

Lin, K. W., Yakymovych, I., Jia, M., Yakymovych, M., & Souchelnytskyi, S. (2010). Phosphorylation of eEF1A1 at Ser300 by TbetaR-I results in inhibition of mRNA translation. *Current Biology*, *20*, 1615–1625.

Lippe, W. R., Steward, O., & Rubel, E. W. (1980). The effect of unilateral basilar papilla removal upon nuclei laminaris and magnocellularis of the chick examined with [3H]2-deoxy-D-glucose autoradiography. *Brain Research*, *196*, 43–58.

Lu, R., Wang, H., Liang, Z., Ku, L., O'Donnell, W. T., Li, W., ... Feng, Y. (2004a). The fragile X protein controls microtubule-associated protein 1B translation and microtubule stability in brain neuron development. *Proceedings of the National Academy of Sciences of the United States of America*, *101*, 15201–15206.

Lu, Y., Monsiavis, P., Tempel, B. L., & Rubel, E. W. (2004b). Activity-dependent regulation of the potassium channel subunits Kv1.1 and Kv3.1. *Journal of Comparative Neurology*, *470*, 93–106.

Martin, K. C., & Zukin, R. S. (2006). RNA trafficking and local protein synthesis in dendrites: An overview. *Journal of Neuroscience*, *26*, 7131–7134.

Mateyak, M. K., & Kinzy, T. G. (2010). eEF1A: Thinking outside the ribosome. *Journal of Biological Chemistry*, *285*, 21209–21213.

McBride, E. G., Rubel, E. W., & Wang, Y. (2013). Afferent regulation of chicken auditory brainstem neurons: Rapid changes in phosphorylation of elongation factor 2. *Journal of Comparative Neurology*, *521*, 1165–1183.

Morrissey, C., Schwefel, D., Ennis-Adeniran, V., Taylor, I. A., Crow, Y. J., & Webb, M. (2015). The eukaryotic elongation factor eEF1A1 interacts with SAMHD1. *Biochemical Journal*, *466*, 69–76.

Neil, M. A., Juskaitis, R., & Wilson, T. (1997). Method of obtaining optical sectioning by using structured light in a conventional microscope. *Optics Letters*, *22*, 1905–1907.

Neil, M. A., Squire, A., Juskaitis, R., Bastiaens, P. I., & Wilson, T. (2000). Wide-field optically sectioning fluorescence microscopy with laser illumination. *Journal of Microscopy*, *197*, 1–4.

Paglini, G., Pigino, G., Kunda, P., Morfini, G., Maccioni, R., Quiroga, S., ... Cáceres, A. (1998). Evidence for the participation of the neuron-specific CDK5 activator P35 during laminin-enhanced axonal growth. *Journal of Neuroscience*, *18*(23), 9858–9869.

Penagarikano, O., Mulle, J. G., & Warren, S. T. (2007). The pathophysiology of fragile x syndrome. *Annual Review of Genomics and Human Genetics*, *8*, 109–129.

Rosenblum, K., Meiri, N., & Dudai, Y. (1993). Taste memory: The role of protein synthesis in gustatory cortex. *Behavioral and Neural Biology*, *59*, 49–56.

Rotschafer, S. E., & Razak, K. A. (2014). Auditory processing in fragile x syndrome. *Frontiers in Cellular Neuroscience*, *8*, 19.

Santoro, M. R., Bray, S. M., & Warren, S. T. (2012). Molecular mechanisms of fragile X syndrome: A twenty-year perspective. *Annual Review of Pathology*, *7*, 219–245.

Serwin, M. (2012). Nuclear Localization of N-Ethylamaleimide Sensitive Factor (Master's thesis). Cell and System Biology, University of Toronto.

Sharma, V., Eng, J. K., MacCoss, M. J., & Riffle, M. (2012). A mass spectrometry proteomics data management platform. *Molecular & Cellular Proteomics*, *11*, 824–831.

Sorensen, S. A., & Rubel, E. W. (2006). The level and integrity of synaptic input regulates dendrite structure. *Journal of Neuroscience*, *26*, 1539–1550.

Sorensen, S. A., & Rubel, E. W. (2011). Relative input strength rapidly regulates dendritic structure of chick auditory brainstem neurons. *Journal of Comparative Neurology*, *519*, 2838–2851.

Stankiewicz, T. R., & Linseman, D. A. (2014). Rho family GTPases: Key players in neuronal development, neuronal survival, and neurodegeneration. *Frontiers in Cellular Neuroscience*, *8*, 314.

Steward, O., & Falk, P. M. (1985). Polyribosomes under developing spine synapses: Growth specializations of dendrites at sites of synaptogenesis. *Journal of Neuroscience Research*, *13*, 75–88.

Steward, O., Farris, S., Pirbhoy, P. S., Darnell, J., & Driesche, S. J. (2014). Localization and local translation of Arc/Arg3.1 mRNA at synapses: Some observations and paradoxes. *Frontiers in Molecular Neuroscience*, *7*, 101.

Tabb, D. L., Vega-Montoto, L., Rudnick, P. A., Variyath, A. M., Ham, A. J., Bunk, D. M., ... Spiegelman, C. (2010). Repeatability and reproducibility in proteomic identifications by liquid chromatography-tandem mass spectrometry. *Journal of Proteome Research*, *9*(2), 761–776.

Verpelli, C., Piccoli, G., Zibetti, C., Zanchi, A., Gardoni, F., Huang, K., ... Sala, C. (2010). Synaptic activity controls dendritic spine morphology by modulating eEF2-dependent BDNF synthesis. *Journal of Neuroscience*, *30*, 5830–5842.

Wang, Y., & Rubel, E. W. (2008). Rapid regulation of microtubule-associated protein 2 in dendrites of nucleus laminaris of the chick following deprivation of afferent activity. *Neuroscience*, *154*, 381–389.

Wang, Y., Cunningham, D. E., Tempel, B. L., & Rubel, E. W. (2009). Compartment-specific regulation of plasma membrane calcium ATPase type 2 in the chick auditory brainstem. *Journal of Comparative Neurology*, *514*, 624–640.

Wang, Y., & Rubel, E. W. (2012). In vivo reversible regulation of dendritic patterning by afferent input in bipolar auditory neurons. *Journal of Neuroscience*, *32*, 11495–11504.

Wang, Y., Sakano, H., Beebe, K., Brown, M. R., de Laat, R., Bothwell, M., ... Rubel, E. W. (2014). Intense and specialized dendritic localization of the fragile X mental retardation protein in binaural brainstem neurons: A comparative study in the alligator, chicken, gerbil, and human. *Journal of Comparative Neurology*, *522*, 2107–2128.

Wang, B., Pan, L., Wei, M., Wang, Q., Liu, W. W., Wang, N., ... Bao, L. (2015). FMRP-Mediated axonal delivery of miR-181d regulates axon elongation by locally targeting Map1b and Calm1. *Cell Reports*, *13*, 2794–2807.

Zalfa, F., Giorgi, M., Primerano, B., Moro, A., Di Penta, A., Reis, S., ... Bagni, C. (2003). The fragile X syndrome protein FMRP associates with BC1 RNA and regulates the translation of specific mRNAs at synapses. *Cell*, *112*, 317–327.

Zarnescu, D. C., Shan, G., Warren, S. T., & Jin, P. (2005). Come FLY with us: Toward understanding fragile X syndrome. *Genes, Brain and Behavior*, *4*, 385–392.

Zhang, B., Chambers, M. C., & Tabb, D. L. (2007). Proteomic parsimony through bipartite graph analysis improves accuracy and transparency. *Journal of Proteome Research*, *6*, 3549–3557.

SUPPORTING INFORMATION

Additional Supporting Information may be found online in the supporting information tab for this article

---